

Negative Sequence Effects on Generator Rotors

Model Details

Negative Sequence Effects on Generator Rotors

Model Details

1015671

Final Report, January 2009

EPRI Project Manager
J. Stein

DISCLAIMER OF WARRANTIES AND LIMITATION OF LIABILITIES

THIS DOCUMENT WAS PREPARED BY THE ORGANIZATION(S) NAMED BELOW AS AN ACCOUNT OF WORK SPONSORED OR COSPONSORED BY THE ELECTRIC POWER RESEARCH INSTITUTE, INC. (EPRI). NEITHER EPRI, ANY MEMBER OF EPRI, ANY COSPONSOR, THE ORGANIZATION(S) BELOW, NOR ANY PERSON ACTING ON BEHALF OF ANY OF THEM:

(A) MAKES ANY WARRANTY OR REPRESENTATION WHATSOEVER, EXPRESS OR IMPLIED, (I) WITH RESPECT TO THE USE OF ANY INFORMATION, APPARATUS, METHOD, PROCESS, OR SIMILAR ITEM DISCLOSED IN THIS DOCUMENT, INCLUDING MERCHANTABILITY AND FITNESS FOR A PARTICULAR PURPOSE, OR (II) THAT SUCH USE DOES NOT INFRINGE ON OR INTERFERE WITH PRIVATELY OWNED RIGHTS, INCLUDING ANY PARTY'S INTELLECTUAL PROPERTY, OR (III) THAT THIS DOCUMENT IS SUITABLE TO ANY PARTICULAR USER'S CIRCUMSTANCE; OR

(B) ASSUMES RESPONSIBILITY FOR ANY DAMAGES OR OTHER LIABILITY WHATSOEVER (INCLUDING ANY CONSEQUENTIAL DAMAGES, EVEN IF EPRI OR ANY EPRI REPRESENTATIVE HAS BEEN ADVISED OF THE POSSIBILITY OF SUCH DAMAGES) RESULTING FROM YOUR SELECTION OR USE OF THIS DOCUMENT OR ANY INFORMATION, APPARATUS, METHOD, PROCESS, OR SIMILAR ITEM DISCLOSED IN THIS DOCUMENT.

ORGANIZATION(S) THAT PREPARED THIS DOCUMENT

Rensselaer Polytechnic Institute

NOTE

For further information about EPRI, call the EPRI Customer Assistance Center at 800.313.3774 or e-mail askepri@epri.com.

Electric Power Research Institute, EPRI, and TOGETHER...SHAPING THE FUTURE OF ELECTRICITY are registered service marks of the Electric Power Research Institute, Inc.

Copyright © 2009 Electric Power Research Institute, Inc. All rights reserved.

CITATIONS

This report was prepared by

Rensselaer Polytechnic Institute
Electrical, Computer and Systems Engineering
Troy, NY 12180-3590

Principal Investigator
S. Salon

This report describes research sponsored by the Electric Power Research Institute (EPRI).

The report is a corporate document that should be cited in the literature in the following manner:

Negative Sequence Effects on Generator Rotors: Model Details. EPRI, Palo Alto, CA: 2009.
1015671.

REPORT SUMMARY

This report is the second part of a study of the effects of severe negative sequence events on round rotor turbine generators. The first part (EPRI report 1014910) introduced simplified models to investigate the thermal and mechanical stresses resulting from unbalanced short circuits and other events. The current report provides documentation on these simplified models. It also describes further studies of the retaining ring and introduces additional models for the pole face and cross-slot regions.

Background

Main generator rotors are constructed and designed to provide decades of reliable and trouble-free operation. However, a number of negative sequence and motoring incidences have occurred over the years that can adversely impact reliable operation of generator rotors and, ultimately, production of electrical power. Severe overheating leads to rotor material changes, such as steel hardness, and may if not detected, ultimately lead to catastrophic failure. This project addressed the effects of severe negative sequence events on round rotor turbine generators.

Objectives

- To document simplified models developed to study the effects of severe negative sequence events on round motor turbine generators
- To apply the simplified models to episodes of motoring

Approach

The project team documented the simplified models for the sunken wedge, retaining ring, and flex slot region introduced in the first part of the study and continued their earlier work by describing additional modeling of the effects of negative sequence events on the retaining ring of round motor turbine generators. The team discussed the application of the models to the analysis of motoring in generators.

Results

This report documents the models that were developed in the first phase of the project for the flush wedge and the sunken wedge configurations. It also includes documentation for the retaining ring model and the flex slot region. A section gives a full development of the one-dimensional nonlinear analysis that is used to calculate the impedance of the tooth and pole face and find the losses. The report also includes the details of the nonlinear iron eddy current equations used in this modeling work. There is also a discussion of motoring and the applicability of the simplified models to motoring operation.

This project provides a method for assessing turbine generator rotors following a negative sequence event. While mechanical stress due to thermal expansion and the potential for arcing

have also been studied, the method is primarily designed to determine hot spot temperatures in the rotor. Arcing damage requires further research. The methods described in this report are most accurate for faults with short durations, where thermal convection to the air gap and conduction deep into the rotor do not significantly affect the results. Where possible, the simplified models have been verified with the finite element method.

EPRI Perspective

The ultimate goal of this project is to provide users with operational recommendations following a significant negative sequence event, such as generator motoring. The "inspect now or later" recommendation will be based on the risk of generator rotor component overheating.

Keywords

Turbines

Generators

Turbine Generator Rotors

Negative Sequence Effects

ABSTRACT

This is part 2 of a study on Negative Sequence Current in generators and their effects on turbine generator rotors. In this report, further studies of the retaining ring are given. Models are introduced for the pole face and cross slot regions. Further documentation is given on all of the simplified models such as slot and wedge combinations, retaining ring, flex slot and pole face. Details of the nonlinear iron eddy current equations are included.

CONTENTS

- 1 INTRODUCTION 1-1**
- 2 RETAINING RING STUDIES.....2-1**
- 3 DESCRIPTION OF THE SIMPLIFIED MODELS: FORMULAS AND SOLUTION METHODS3-1**
 - 3.1 Simplified Model for the Sunken Wedge 3-4
 - 3.1.1 Summary of Equations for the Sunken Wedge Model..... 3-8
 - 3.1.2 Pole Face Region 3-12
 - 3.1.3 Transient Temperature Simplified Model for Two Node Circuit..... 3-14
 - 3.2 Analysis of the Depth to which the Heat diffuses in a given Time 3-18
 - 3.3 Retaining Ring..... 3-20
 - 3.4 Model for the Flex Slot Region Based on Electric Conduction..... 3-24
 - 3.4.1 Temperature of the Flex Slot 3-29
- 4 APPLYING THE SIMPLIFIED MODELS TO MOTORING 4-1**
- 5 SUMMARY AND CONCLUSIONS 5-1**
- A EDDY CURRENTS IN STEEL A-1**
 - A.1 Losses A-7
 - A.2 Losses in Nonlinear Steel A-10

LIST OF FIGURES

Figure 2-1 Rotor, retaining ring, and slot with ideal surface contacts	2-2
Figure 2-2 Partial impedance surface extending from slot, $\rho = 2.4E - 7\Omega/m$	2-3
Figure 2-3 Partial impedance surface extending from slot, $\rho = 1.0E - 5\Omega/m$	2-4
Figure 3-1 Impedance surface from slot to corner, $\rho = 1.0E - 6\Omega/m$	3-1
Figure 3-2 Equivalent circuit for shrink fit and result	3-2
Figure 3-3 Current in the 2 branches of the shrink fit model.....	3-2
Figure 3-4 Currents through the wedge and the steel, respectively, when a large contact resistance between the steel and the retaining ring. The contact resistance between the wedge and the retaining ring is variable.....	3-3
Figure 3-5 Currents through the wedge and the steel, respectively, when the contact resistance between the steel and retaining ring is small. The contact resistance between the wedge and the retaining ring is variable	3-4
Figure 3-6 Model of the sunken wedge.....	3-5
Figure 3-7 Tooth dimensions	3-5
Figure 3-8 Equivalent circuit for sunken wedge	3-6
Figure 3-9 Flush wedge geometry	3-10
Figure 3-10 Equivalent circuit flush wedge	3-11
Figure 3-11 One dimensional solid steel (low current).....	3-13
Figure 3-12 One dimensional solid steel (high current)	3-14
Figure 3-13 Ladder network for temperature calculation	3-14
Figure 3-14 Simple 2 node R-C thermal network.....	3-15
Figure 3-15 Transient temperature at different depths	3-19
Figure 3-16 Evaluation of coefficient Ra	3-19
Figure 3-17 Expanded view of retaining ring	3-21
Figure 3-18 Two node retaining ring thermal model	3-22
Figure 3-19 Retaining ring dimensions	3-23
Figure 3-20 Pole face cross slots.....	3-24
Figure 3-21 Rotor wedges	3-25
Figure 3-22 Conduction (resistance) network	3-26
Figure 3-23 Electrical network for the flex slot	3-31
Figure 3-24 Temperature model for the flex slot.....	3-32
Figure 4-1 Generator and governor steady state characteristic.....	4-2

Figure A-1 Limiting B-H curve of steel	A-1
Figure A-2 Making A sinusoidal wave from square waves	A-2
Figure A-3 Separation surface and coordinate system.....	A-4
Figure A-4 Steel cylinder with axial current and skin depth	A-5
Figure A-5 Current density vs depth (low current)	A-11
Figure A-6 Current density vs depth (medium current).....	A-12
Figure A-7 Current density vs depth (high current).....	A-13

1

INTRODUCTION

This report is the second installment of the RPI studies of the negative sequence capability of turbine generator rotors. In the first report¹ the concept of simplified models was introduced and these models were checked with finite element analysis for the losses and resulting temperatures that resulted from the negative sequence component of short circuit current. We also did extensive finite element studies of the mechanical stress that resulted from the thermal differential in the tooth and slot region. We included different assumptions as to the tolerances and fit of the wedge in the slot. It is the differential expansion which produced the thermal induced stress. In our studies although there was a very high thermal gradient, we found that the mechanical stresses induced by this effect were not a problem. The total temperature however could reach values that would affect the mechanical strength of the materials. Total temperature limits have been published by General Electric and Hitachi and these values agree with each other. These are discussed in the earlier report and we continue to use these as upper allowable limits on the total temperature.

In this report we discuss the simplified models of the retaining ring and pole face. There is also a discussion of motoring and the applicability of the simplified models to motoring operation.

One of the main goals of this report is to document the simplified models so that they can be programmed and a reliable maintainable computer program can be written. This report documents of the models that were developed in the first phase of the project for the flush wedge and the sunken wedge configurations. We also include documentation for the retaining ring model and the flex slot region. A section gives a full development of the one dimensional nonlinear analysis that is used to calculate the impedance of the tooth and pole face and find the losses.

¹ *Negative Sequence Effects on Generator Rotors: Basic Principles and Models*. EPRI, Report 1014910.

2

RETAINING RING STUDIES

Previous investigations demonstrated that the current in the magnetic material of the rotor was close to the surface due to the magnetic permeability and the conductivity of the steel. The stainless steel retaining ring is assumed to be only slightly magnetic and has an increased skin depth resulting in current lines that are more distributed throughout the material. The current paths couple closely to the corner junction and diverge as they enter the retaining ring. The slot material has a nominal effect on the current paths, due its relatively large distance from the junction. For the simulation shown, it is assumed that the contact between the retaining ring and the rotor is smooth and continuous. This assumption is useful for establishing an estimate of field and current behavior in first order approximations. Considering geometries as rigid structures, each surface should have three points of contact with a relatively high current density. The simple two dimensional motor model has planar surface contacts between the three materials corresponding to the rotor, the wedge material and the retaining ring. In operation, thermal and mechanical stresses have a significant impact on the junction between the rotor and the retaining ring, which makes accurate determination of the physical characteristics very difficult. By studying the ideal simulation, the effects of the deformation will be of primary significance on the surface between the slot and the corner junction.

In the next series of figures, an impedance surface was introduced to simulate the effects of increased resistance that can occur between the rotor and the retaining ring. Several simulations were performed with varying levels of resistance and various contact points. Estimating the impedance of the surface largely depends on the deformation and whether any contact material is in place. In the first figure 2-1 we assume an ideal contact over the entire region. In the next 2 figures, (Figures 2-2, 2-3) the impedance layer starts a short distance from the corner junction. The corner junction contact still provides a continuous low resistively path for the current as can be seen in the figures and a large current density is seen in this region.

In the figure 3-1, the impedance effect is seen on the complete surface between the rotor and the retaining ring. The effect of the geometry is to spread the current across the junction, reducing the current density in the vicinity of the corner. In the retaining ring, the current paths return to their expected locations. As the resistance of the layer increases, the current is shifted further from the junction. In the extreme case, where an open circuit develops, the current path would be thought he slot material and a sharp discontinuity would exist. In this case, arcing is likely due to the strong field effects.

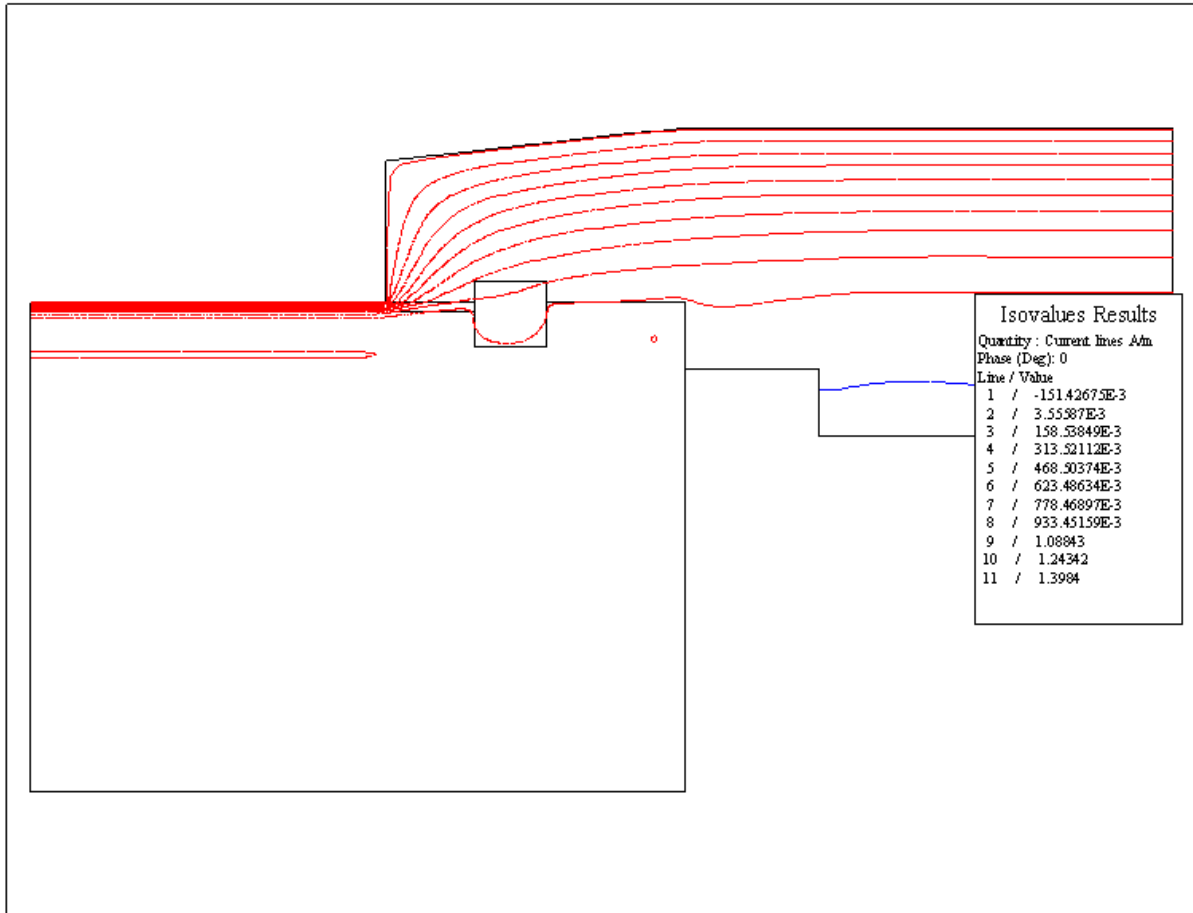


Figure 2-1
Rotor, retaining ring, and slot with ideal surface contacts

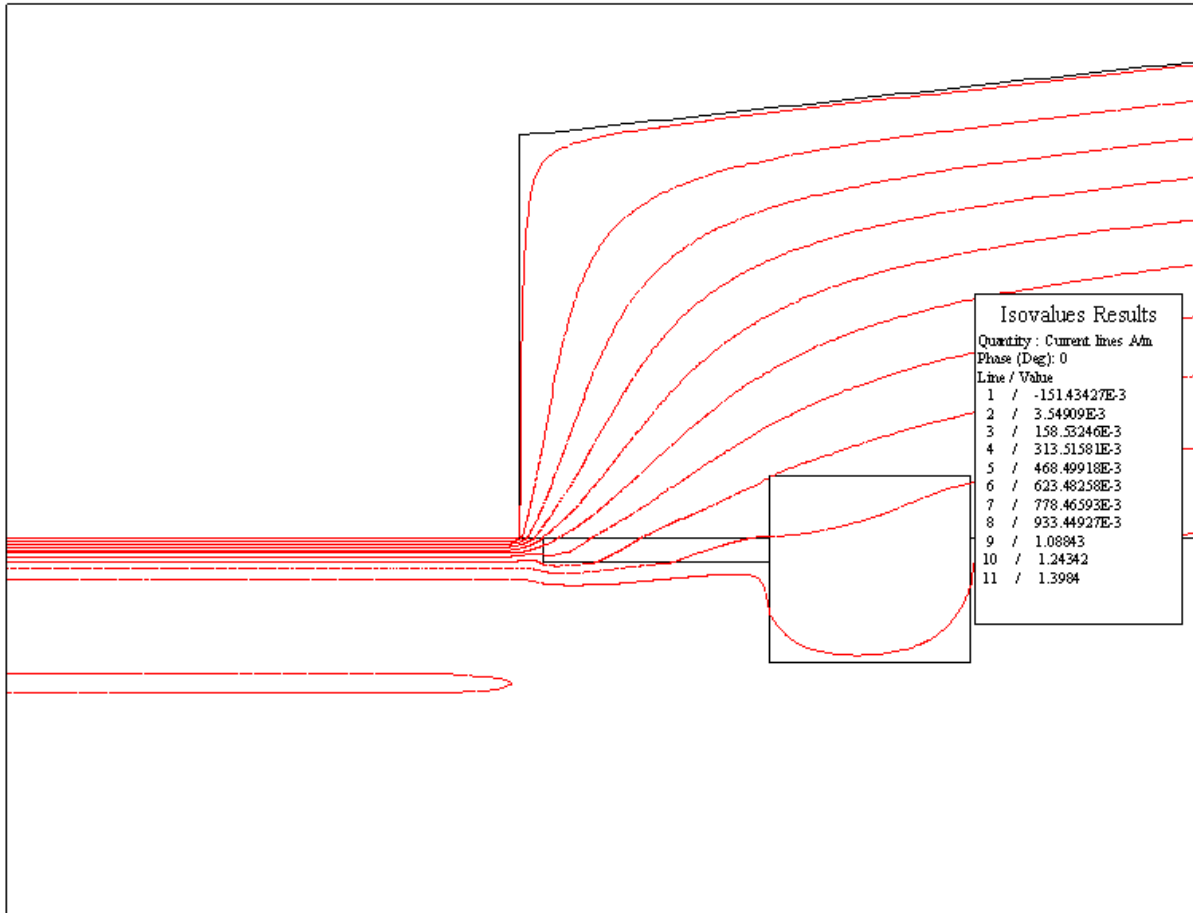


Figure 2-2
Partial impedance surface extending from slot, $\rho = 2.4E - 7\Omega/m$

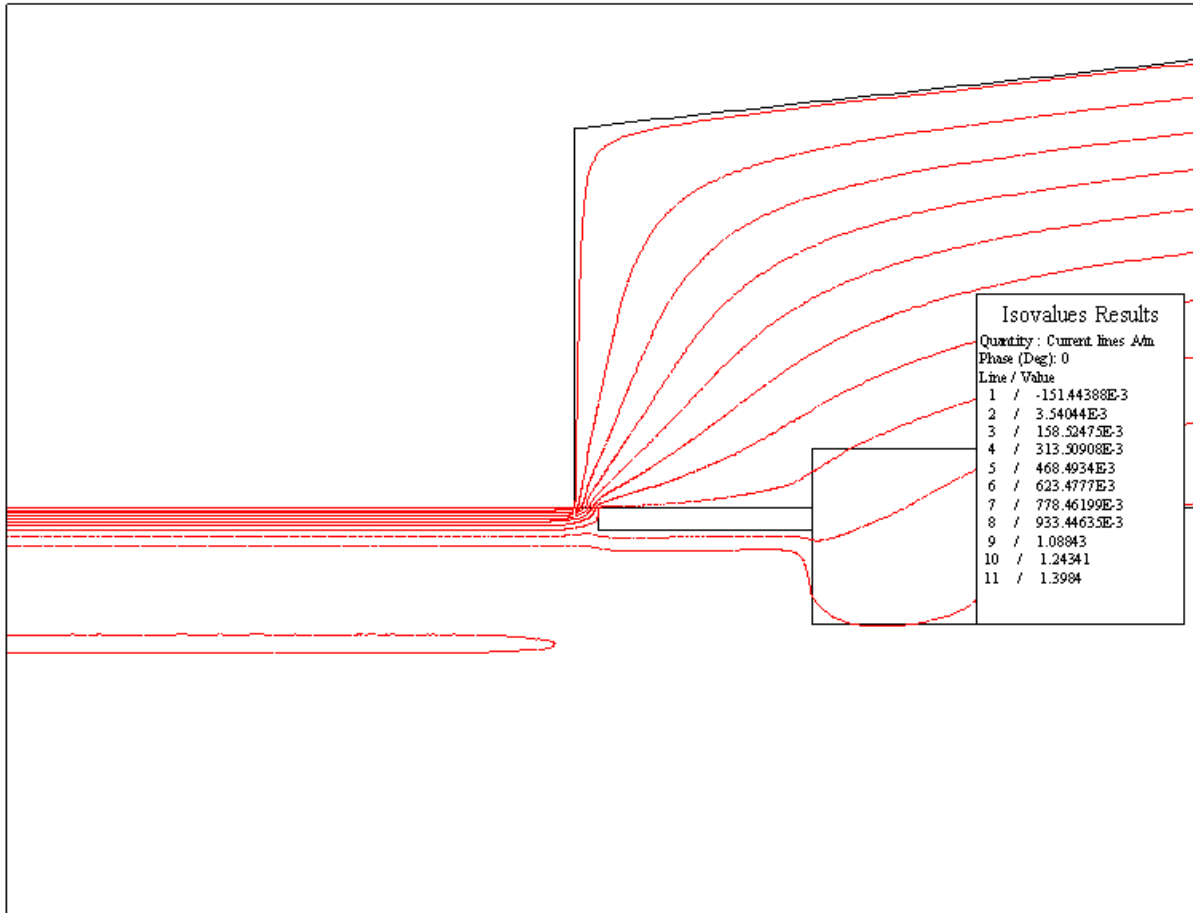


Figure 2-3
Partial impedance surface extending from slot, $\rho = 1.0E - 5\Omega/m$

To model this as a simple circuit, we have chosen two parallel paths in the slot and tooth. The currents can redistribute at the retaining ring shrink fit region depending on the contact resistance and ring impedance. The currents coming down the rotor are the same as used in the half slot models. PSpice simulations were applied to the equivalent circuit connecting the rotor and the retaining ring. When considering the axial current, two possible paths exist, one through the wedge and one through the steel. Both of these materials are in contact with the retaining ring, though, as discussed the contact surface is typically not ideal and can be modeled as a resistance. In the circuit schematic, each material is represented as a resistor and inductor in series. Each surface is modeled as a resistor. In addition the surface between the wedge and the steel is modeled as a contact resistance. Current that moves in this direction is no longer axial, which requires including the inductive effect. The equivalent circuit used is illustrated in Figure 3-2. The current through the wedge section and the tooth section found from this model is shown in Figure 3-3.

As discussed previously, the effects of the contact resistance can be significant. In the following figures, the contact resistance between the rotor and the retaining ring is varied for the two possible current paths. In Figure 3-4, the currents through the wedge and the steel are shown for varying contact resistances between the wedge and the retaining ring. In these simulations, the contact resistance between the steel and the retaining ring is significant. As expected, low contact resistances between the wedge and the retaining ring results in a low impedance path. When the contact resistances between both materials and the retaining ring are comparable, the currents are more evenly split between the two paths. The results in Figure 3-5 demonstrate a similar situation, except the contact resistance between the steel and the retaining ring is negligible. As expected, this path is favorable if the contact resistance between the wedge and the retaining ring is significant. Similarly, the current becomes more evenly distributed as the contact resistance between the wedge and the retaining ring becomes negligible.

In order for significant current to move between the wedge and the steel, the contact resistance between those materials and the retaining ring must be significantly different. Given the nature of the geometry, the contact resistance between the wedge and the steel is likely small. This is demonstrated in Figure 3-5 by the relatively stable curves. Only in the event that a large contact resistance develops does a small current move from the wedge to steel.

3

DESCRIPTION OF THE SIMPLIFIED MODELS: FORMULAS AND SOLUTION METHODS

In this section we present the expressions necessary to evaluate the parameters in the simplified models. We also include the strategy for solution. Most of the models are nonlinear and they must be solved iteratively. In the case of the electromagnetic and loss evaluation calculations, the analysis is complex phasor analysis. In the case of the thermal models, the results are in the time domain. The models below are the models for the sunken wedge, the flush wedge, the pole face, the retaining ring, and the flexibility slot region.

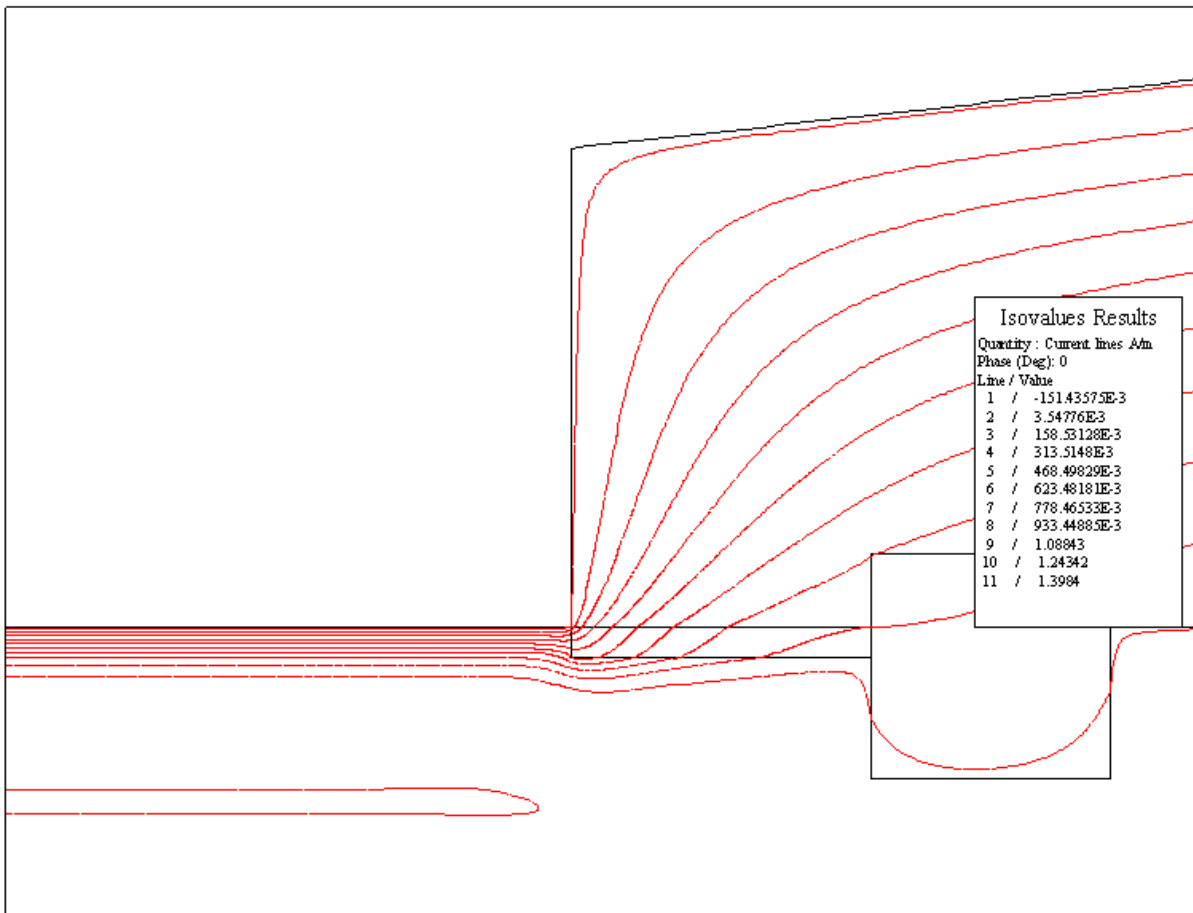


Figure 3-1
Impedance surface from slot to corner, $\rho = 1.0E - 6\Omega/m$

Equivalent Circuit

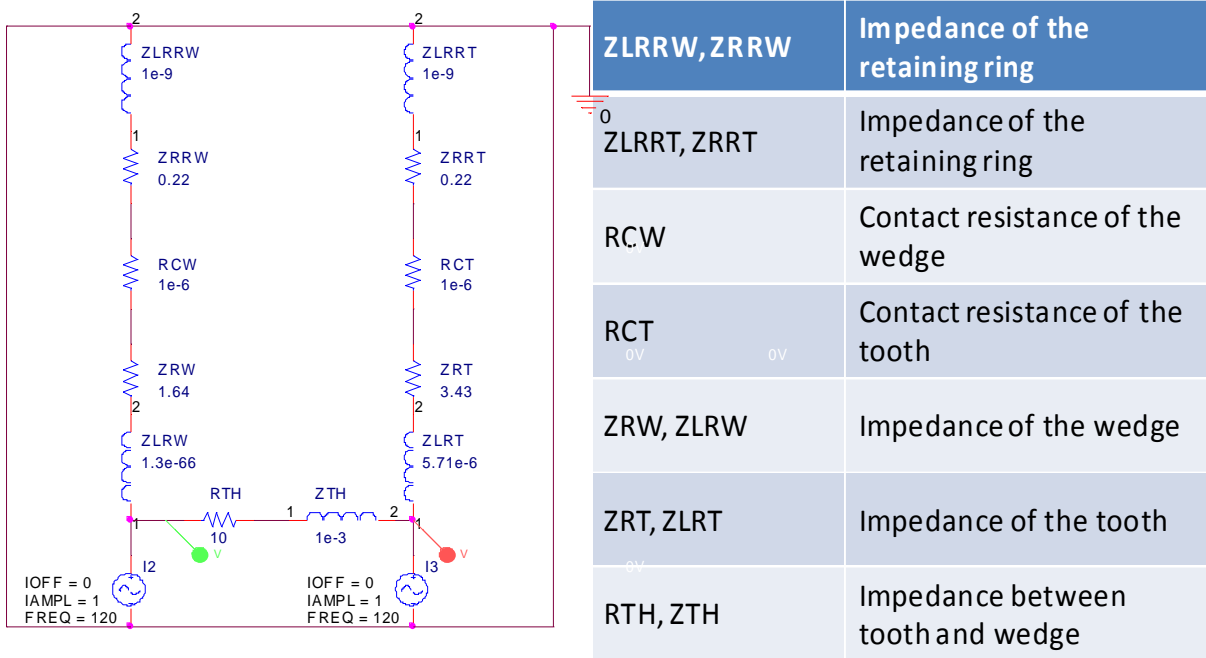


Figure 3-2
Equivalent circuit for shrink fit and result



Figure 3-3
Current in the 2 branches of the shrink fit model

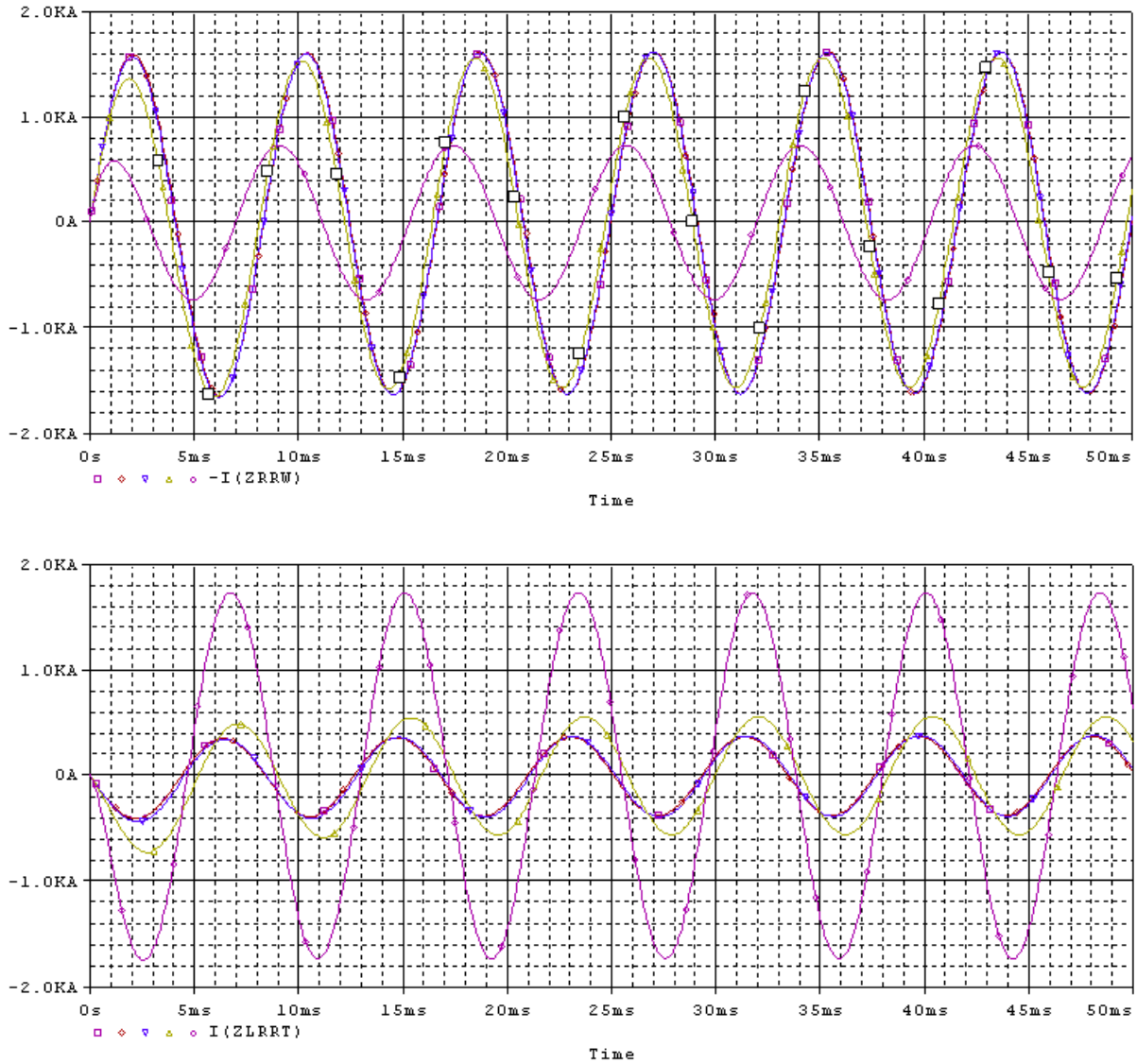


Figure 3-4
Currents through the wedge and the steel, respectively, when a large contact resistance between the steel and the retaining ring. The contact resistance between the wedge and the retaining ring is variable

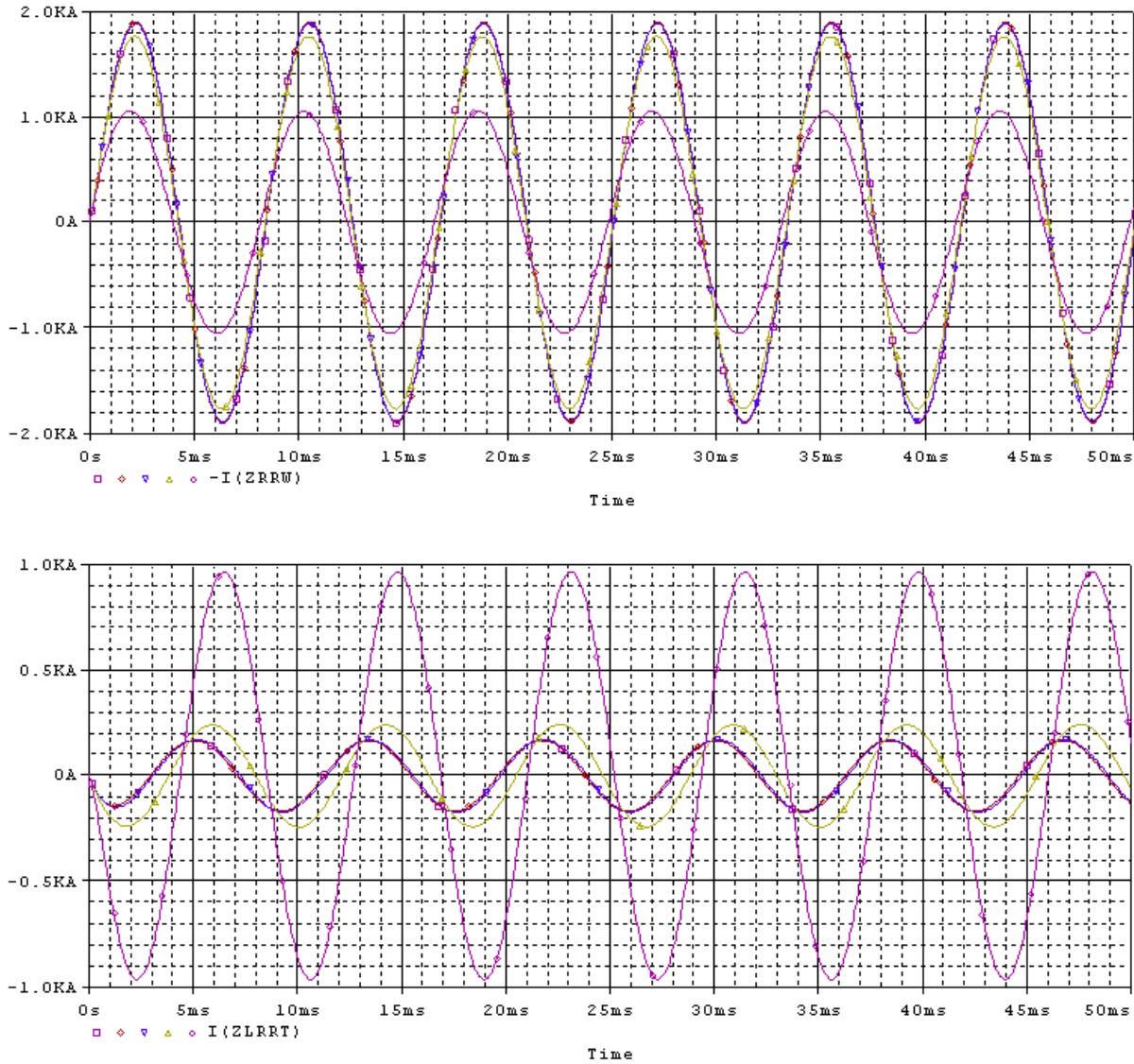


Figure 3-5
Currents through the wedge and the steel, respectively, when the contact resistance between the steel and retaining ring is small. The contact resistance between the wedge and the retaining ring is variable

3.1 Simplified Model for the Sunken Wedge

The figure below (Figure 3-6) shows the model for the sunken wedge. The model is for one half slot. We take the center line of the tooth and center line of the slot as symmetry planes. This is described in the first report. We ignore the field winding effect in this model since it is too deep to carry much of the negative sequence current. This has been confirmed by finite element analysis.

The effective resistance and reactance of the tooth in this configuration included the side of the tooth above the wedge height. The effective surface area of the tooth is one parameter in the model. The effective area is shown in Figure 3-7.

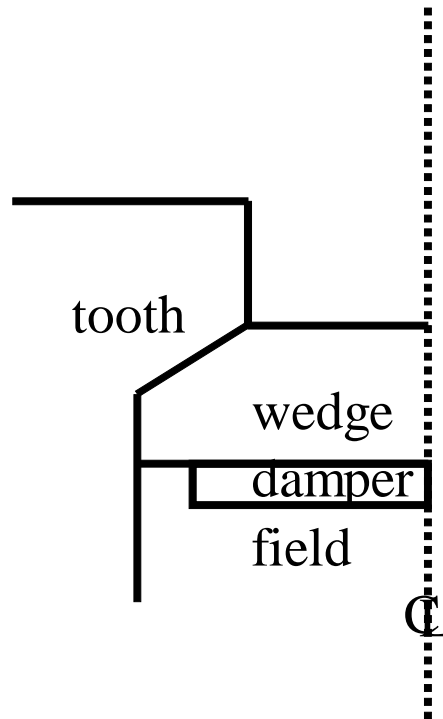


Figure 3-6
Model of the sunken wedge

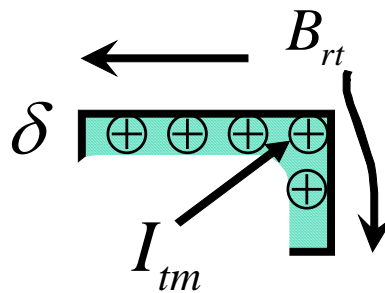


Figure 3-7
Tooth dimensions

Figure 3-8 below shows the model for the sunken wedge. This is based on the magnetic vector potential finite difference formulation of the eddy current equation. The permeances are a function of the geometry and the magnetic permeability of each of the regions. There is one for the air gap region above the tooth and slot, one for the wedge and one for the damper. There is one for the tooth region. The capacitance in the model are the eddy current paths. The model represents the currents in the damper bar, the wedge, and the tooth. The eddy currents in the tooth are described by the limiting nonlinear analysis described further down in this report.

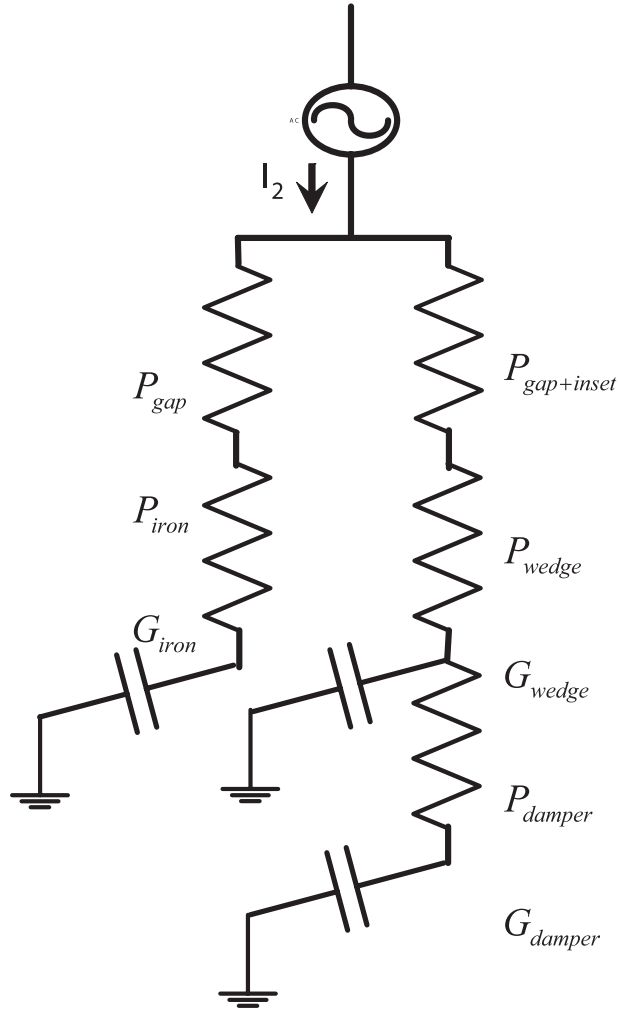


Figure 3-8
Equivalent circuit for sunken wedge

The right hand side of the circuit will now be simplified. In this model the magnetic permeances are represented by resistors and the conductances are represented by capacitances.

First referring to equations (3-1 - 3-3)

$$Z_d = P_{wd} - \frac{1}{\omega G_w} \quad \text{Equation 3-1}$$

$$Z_w = -\frac{j}{\omega G_w} \quad \text{Equation 3-2}$$

$$Z_{dw} = \frac{Z_d Z_w}{Z_d + Z_w} \quad \text{Equation 3-3}$$

Now

$$Z_d + Z_w = P_{wd} - \frac{1}{\omega} \left(\frac{1}{G_d} + \frac{1}{G_w} \right) \quad \text{Equation 3-4}$$

Calling the term in parenthesis R_{dw}

Let

$$D = P_{wd}^2 + \left(\frac{R_{dw}}{\omega} \right)^2 \quad \text{Equation 3-5}$$

Breaking this up into real and imaginary components

$$Br = \frac{R_{dw} P_{wd}}{\omega^2 G_d G_w} \quad \text{Equation 3-6}$$

$$Bi = \frac{P_{wd}^2}{\omega G_w} + \frac{R_{dw}}{\omega^3 G_d G_w} \quad \text{Equation 3-7}$$

So

$$Z_{dw} = \frac{Br}{D} - j \frac{Bi}{D} = PE + jXE \quad \text{Equation 3-8}$$

and

$$ZR = Z_{dw} + P_{gs} = P_{gs} + PE - jXE \quad \text{Equation 3-9}$$

Now for the left hand side of the circuitto find ZL

$$ZL = P_{gi} = \frac{j}{\omega G_L} = PGI - jXGI \quad \text{Equation 3-10}$$

We now find the division of the current $I_{sp1} \angle 0$ into tooth current, I_t and wedge current I_w .

$$I_t = \frac{ZR}{ZR + ZL} I_{sp1} \quad \text{Equation 3-11}$$

$$I_w = \frac{ZL}{ZR + ZL} I_{sp1}$$

Now we evaluate the denominator as in (3-12)

$$ZL + ZR = P_{gi} + PE_t - j(X_{gi} + XE) = P_{\phi t} - jX_{\phi t} \quad \text{Equation 3-12}$$

3.1.1 Summary of Equations for the Sunken Wedge Model

We can now summarize the equations used

$$\omega = 2\pi f \quad \text{Equation 3-13}$$

$$R_{dw} = \frac{1}{G_d} + \frac{1}{G_w} \quad \text{Equation 3-14}$$

$$D = P_{wd}^2 + \left(\frac{P_{dw}}{\omega} \right)^2 \quad \text{Equation 3-15}$$

$$BR = \frac{P_{wd}}{\omega^2 G_w} \left(R_{dw} - \frac{1}{G_d} \right) \quad \text{Equation 3-16}$$

$$BI = \frac{1}{\omega G_w} \left(P_{wd}^2 + \frac{R_{dw}}{\omega^2 G_d} \right) \quad \text{Equation 3-17}$$

$$PE = \frac{BR}{D} \quad \text{Equation 3-18}$$

$$XE = \frac{BI}{D} \quad \text{Equation 3-19}$$

$$PET = P_{gs} + PE \quad \text{Equation 3-20}$$

$$PGI = P_{gi} \quad \text{Equation 3-21}$$

$$XGI = \frac{1}{\omega G_i} \quad \text{Equation 3-22}$$

$$Dm = \sqrt{P_{wd}^2 + \left(\frac{R_{dw}}{\omega} \right)^2} \quad \text{Equation 3-23}$$

$$\theta_{\phi d} = \tan^{-1} \left(\frac{-R_{dw} / \omega}{P_{wd}} \right) \quad \text{Equation 3-24}$$

$$P_{\phi t} = P_{gi} + P_{Et} \quad \text{Equation 3-25}$$

$$X_{\phi t} = X_{gi} + XE \quad \text{Equation 3-26}$$

$$DTM = \sqrt{P_{\phi t}^2 + X_{\phi t}^2} \quad \text{Equation 3-27}$$

$$\theta_{\phi} = \tan^{-1} \frac{-X_{\phi t}}{P_{\phi t}} \quad \text{Equation 3-28}$$

$$ZRM = \sqrt{P_{et}^2 + XE^2} \quad \text{Equation 3-29}$$

$$\theta_R = \tan^{-1} \frac{XE}{P_{et}} \quad \text{Equation 3-30}$$

$$ZLM = \sqrt{P_{gi}^2 + X_{gi}^2} \quad \text{Equation 3-31}$$

$$\theta_L = \tan^{-1} \frac{X_{gi}}{P_{gi}} \quad \text{Equation 3-32}$$

$$ZDM = \sqrt{P_{wd}^2 + \left(\frac{1}{\omega G_d}\right)^2} \quad \text{Equation 3-33}$$

$$\theta_{Dx} = \tan^{-1} \frac{\left(\frac{-1}{\omega G_d}\right)}{P_{wd}} \quad \text{Equation 3-34}$$

We can now find the currents as follows

The tooth currents is

$$I_t \angle \theta_t = \frac{ZRM \angle \theta_R}{DTM \angle \theta_\phi} \quad \text{Equation 3-35}$$

The wedge and damper currents is

$$I_w \angle \theta_w = \frac{ZLM \angle \theta_L}{DTM \angle \theta_\phi} \quad \text{Equation 3-36}$$

The damper bar current is

$$I_D \angle \theta_D = \frac{\frac{1}{\omega G_w} \angle 90^\circ}{DM \angle \theta_{\phi D}} \quad \text{Equation 3-37}$$

The wedge current is

$$I_{wp} \angle \theta_{wp} = \frac{ZDM \angle \theta_{Dx}}{DM \angle \theta_{\phi D}} \quad \text{Equation 3-38}$$

The currents are now used to find the losses for the transient temperature calculation.

$$WT = K\phi \times I_t^{3/2} \quad \text{Equation 3-39}$$

$$WD = \frac{I_D^2}{G_D} \quad \text{Equation 3-40}$$

$$WWP = \frac{I_{wp}^2}{G_w} \quad \text{Equation 3-41}$$

$$WW = WD + WWP \quad \text{Equation 3-42}$$

$$K\phi = 2.54 \times 10^{-4} \sqrt{\frac{g_i B_s f}{BRT}} \quad \text{Equation 3-43}$$

Now we consider the flush wedge geometry. The geometry is illustrated in the figure below (Figure 3-9). The geometry is similar to the sunken wedge but with the difference that there is an extra air gap over the wedge and the tooth has a larger area expose to the gap.

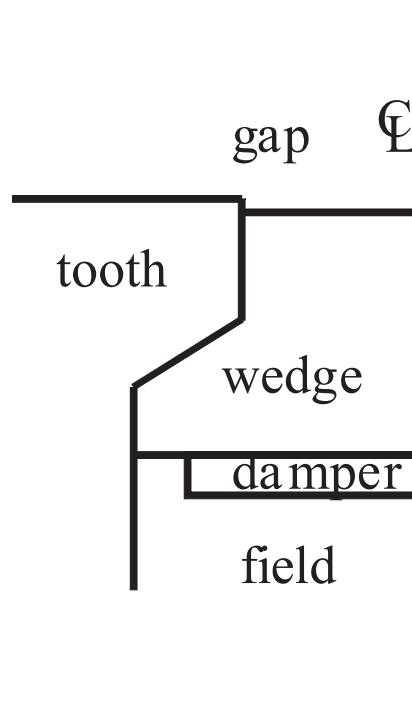


Figure 3-9
Flush wedge geometry

The equivalent circuit is shown below in Figure 3-10. It is also similar to the sunken wedge case.

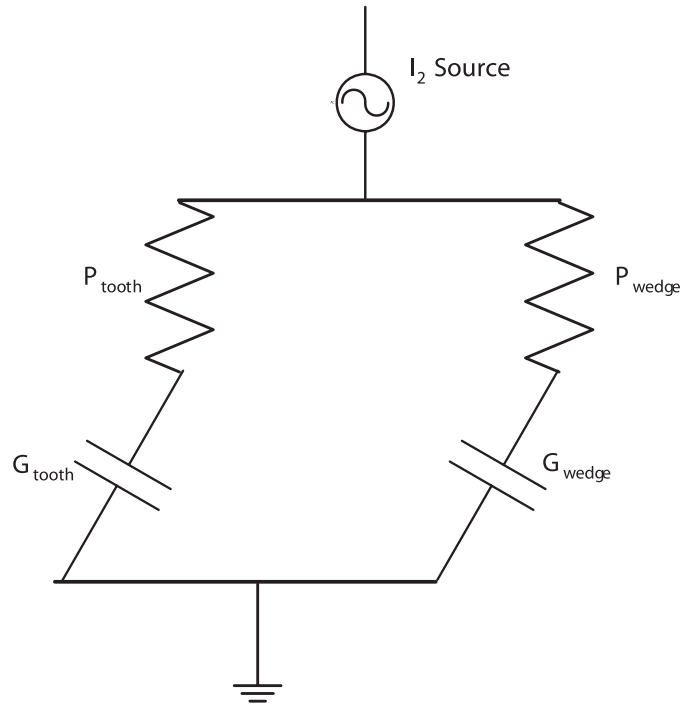


Figure 3-10
Equivalent circuit flush wedge

The equations for the flush wedge case are similar to the sunken wedge case.

The equation are given below as equations 3-44-3-54.

$$\omega = 2\pi f \quad \text{Equation 3-44}$$

$$XR = \frac{1}{\omega G_w} \quad \text{Equation 3-45}$$

$$XL = \frac{1}{\omega G_i} \quad \text{Equation 3-46}$$

$$ZRM = \sqrt{P_{gs}^2 + XR^2} \quad \text{Equation 3-47}$$

$$\theta_R = \tan^{-1} \frac{XR}{P_{gs}} \quad \text{Equation 3-48}$$

$$ZLM = \sqrt{P_{gi}^2 + XL^2} \quad \text{Equation 3-49}$$

$$\theta_L = \tan^{-1} \frac{XL}{P_{gs}} \quad \text{Equation 3-50}$$

$$P_{\phi t} = P_{gi} + P_{gs} \quad \text{Equation 3-51}$$

$$X_{\phi_t} = XL + XR \quad \text{Equation 3-52}$$

$$DTM = \sqrt{P_{\phi_t}^2 + X_{\phi_t}^2} \quad \text{Equation 3-53}$$

$$\theta_{\phi} = \tan^{-1} \frac{X_{\phi_t}}{P_{\phi_t}} \quad \text{Equation 3-54}$$

We now find the currents in the tooth and wedge as

$$I_t = \frac{ZRM \angle \theta_R}{DTM \angle \theta_{\phi}} \quad \text{Equation 3-55}$$

$$I_w = \frac{ZLM \angle \theta_L}{DTM \angle \theta_{\phi}} \quad \text{Equation 3-56}$$

The losses per unit depth (inches) are then

$$WT = K\phi \times I_t^{3/2} \quad \text{Equation 3-57}$$

$$WW = \frac{I_w^2}{G_w} \quad \text{Equation 3-58}$$

$$K\phi = 2.54 \times 10^{-4} \sqrt{\frac{g_i B_s f}{BRT}} \quad \text{Equation 3-59}$$

3.1.2 Pole Face Region

We can view the pole face region as a limiting case of the slotted region. The exception is if we are interested in the flex slots or cross slots that are cut in the direct axis. These are discussed in a separate section below. The pole face is a uniform region of magnetic steel with the current sheet above, producing the negative sequence losses. If we take the slot model and either eliminate the slot portion, i.e. leave only the tooth and make this a uniform region with no hang over, or fill the slot with magnetic steel, we have the pole face model. This is a simple one dimensional model and the limiting nonlinear theory will be applicable. As an example of this model (see Figure 3-11) we use finite element analysis on the slot model with the slot material, normally wedge material, with the tooth material. We ran a number of cases with different currents to check the nonlinear formulation. In the figure below we have 5,000 Amps in the stator current sheet. We see the sharp cut-off of the flux density and the relatively uniform flux density near the surface. The total losses are 39.525 kW.

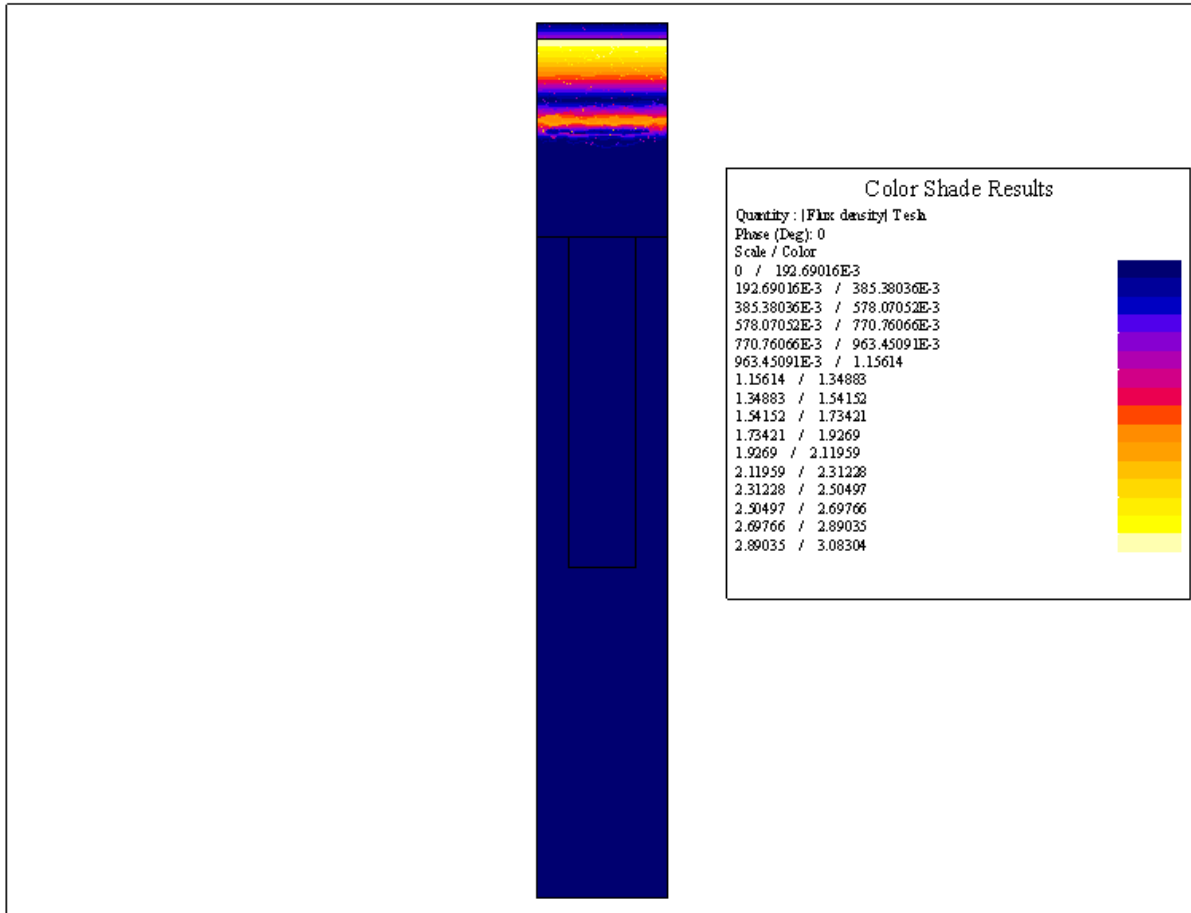


Figure 3-11
One dimensional solid steel (low current)

In the figure below (Figure 3-12), we have the same geometry but the current density is now 5 times greater than in the previous case. From the nonlinear formulation the skin depth should be $\sqrt{5}$ times greater. This appears to be the case. The thermal model is just the same as the model for the slot wedge combinations. We just replace the material for the wedge and replace it with steel or even simpler, eliminate the wedge (set the width to zero or nearly so).

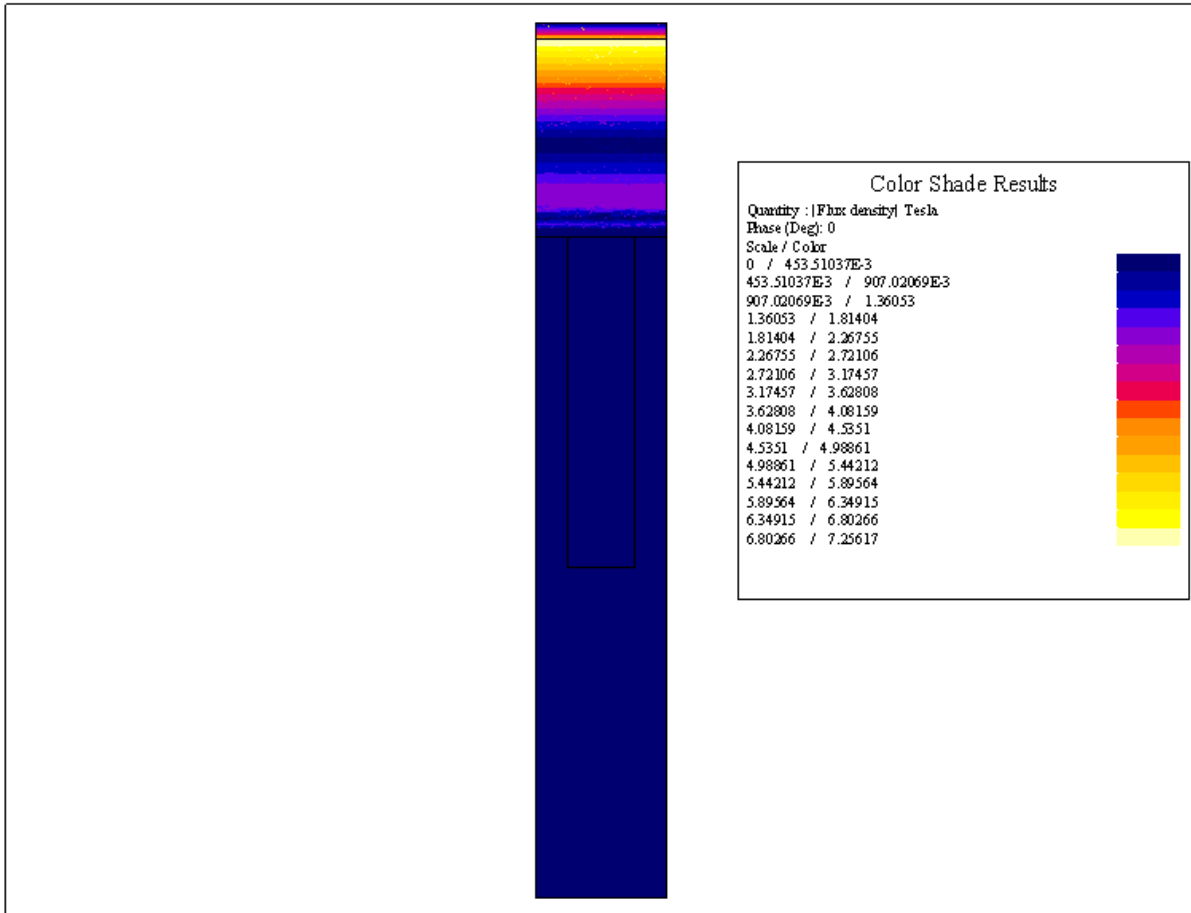


Figure 3-12
One dimensional solid steel (high current)

3.1.3 Transient Temperature Simplified Model for Two Node Circuit

We use the principle that the heat into a volume is equal to the heat out plus the heat stored in the volume. This is equivalent to the finite difference expansion of the heat or diffusion equation. The necessary inputs to the model are the geometry, the loss or loss density and the material properties which are the thermal receptivity (or conductivity) and the specific heat (volume).

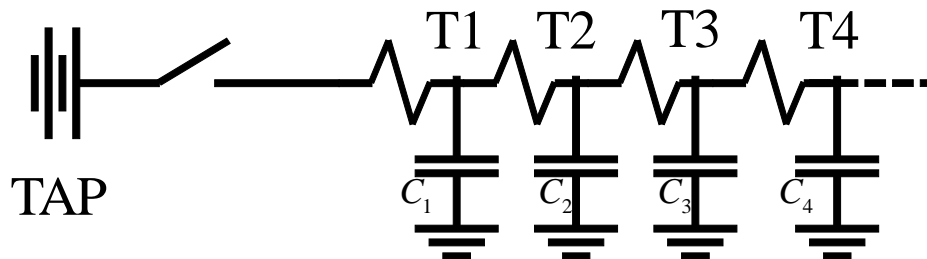


Figure 3-13
Ladder network for temperature calculation

Referring to the equivalent circuit of Figure 3-14 and using $G = \text{conductance} = 1/R$

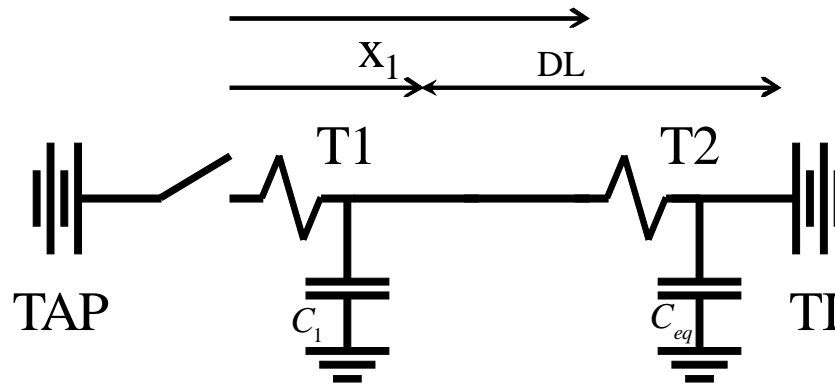


Figure 3-14
Simple 2 node R-C thermal network

we have

$$G1 = C1c + G1A + G12 \quad \text{Equation 3-60}$$

$$G2 = G2B + G2D + G12 \quad \text{Equation 3-61}$$

$$WT1 = W1 + Tba \times G2B + Tbc \times G1c \quad \text{Equation 3-62}$$

$$WT2 = W2 + Tbb \times G2B + Tbd \times G2D \quad \text{Equation 3-63}$$

Note that the boundary temperatures Tbc , Tba , Tbb , and Tbd are always assumed to be known.

We now have two first order ordinary differential equations (equations 3-64 and 3-65)

$$W1 = (T1 - T2) G12 + (T1 - Tba) G1A + (T1 - Tbc) G1c + C1 \frac{dT1}{dt} \quad \text{Equation 3-64}$$

$$W2 = (T2 - T1) G12 + (T2 - Tbb) G2B + (T2 - Tbd) G2D + C2 \frac{dT2}{dt} \quad \text{Equation 3-65}$$

Rearranging these

$$WT1 = T1 \cdot G1 - T2 \cdot G12 + C1 \frac{dT1}{dt} \quad \text{Equation 3-66}$$

$$WT2 = -T1 \cdot G12 + T2 \cdot G2 + C2 \frac{dT2}{dt} \quad \text{Equation 3-67}$$

Where C is the thermal capacitance (specific heat times volume), G is the thermal conductance, W is the heat rate and T is the temperature.

We can solve the equation in a more or less general form.

$$T_n = Ae^{m1t} + Be^{m2t} + T_{nss} \quad \text{Equation 3-68}$$

where T_{nss} is the steady state temperature. We now eliminate T_2 using the Heavyside operator p

$$WT_1 \cdot G_2 + WT_2 \cdot G_{12} = C_1 \cdot C_2 \cdot p^2 T_1 + (C_1 \cdot G_2 + C_2 \cdot G_1) p T_1 + T_1 (G_1 \cdot G_2 - G_{12}^2)$$

Equation 3-69

For the steady state temperature we have

$$WT_1 \cdot G_2 + WT_2 \cdot G_{12} = T_1 (G_1 \cdot G_2 - G_{12}^2)$$

Equation 3-70

$$T_{1ss} = \frac{WT_1 \cdot G_2 - WT_2 \cdot G_{12}}{G_1 \cdot G_2 - G_{12}^2}$$

Equation 3-71

For the exponential we find the characteristic equation

$$m^2 T_1 + \left(\frac{C_1 \cdot G_2 + C_2 \cdot G_1}{C_1 \cdot C_2} \right) m \cdot T_1 + \left(\frac{G_1 \cdot G_2 - G_{12}^2}{C_1 \cdot C_2} \right) = 0$$

Equation 3-72

This is of the form

$$m^2 + bm + c = 0$$

Equation 3-73

So we can solve for m as

$$m_{1,2} = \frac{-b \pm \sqrt{b^2 + 4c}}{2}$$

Equation 3-74

We impose boundary conditions to find the coefficients A and B in equation 3-68.

So

$$T_1 /_{t=0} = T_1 \phi;$$

Equation 3-75

$$T_2 /_{t=0} = T_2 \phi$$

Equation 3-76

and

$$\frac{dT_1}{dt} = \frac{WT_1 + T_2 \phi \cdot G_{12} - T_1 \phi \cdot G_1}{C_1}$$

Equation 3-77

T_2 is now found since we have solved for T_2 in terms of T_1 .

Summary of Equations for the 2 Node Transient Temperature Model are given in equations 3-78 – 3-92.

$$G_1 = G_1 C + G_1 A + G_{12}$$

Equation 3-78

$$G_2 = G_2 B + G_2 D + G_{12}$$

Equation 3-79

$$WT1 = W1 + Tba \cdot G1A + Tbc \cdot G1C \quad \text{Equation 3-80}$$

$$WT2 = W2 + Tbb \cdot G2B + Tbd \cdot G2D \quad \text{Equation 3-81}$$

$$b = \frac{C1 \cdot G2 + C2 \cdot G1}{C1 \cdot C2} \quad \text{Equation 3-82}$$

$$c = \frac{G1 \cdot G2 - G12^2}{C1 \cdot C2} \quad \text{Equation 3-83}$$

$$m_1 = \frac{-b + \sqrt{b^2 - 4c}}{2} \quad \text{Equation 3-84}$$

$$m_2 = \frac{-b - \sqrt{b^2 - 4c}}{2} \quad \text{Equation 3-85}$$

$$DER1 = \frac{WT1 + T2\phi \cdot G2 - T1\phi \cdot G1}{C1} \quad \text{Equation 3-86}$$

$$T1_{ss} = \frac{WT1 \cdot G2 + WT2 \cdot G12}{G1 \cdot G2 - G12^2} \quad \text{Equation 3-87}$$

$$T2_{ss} = \frac{G1 \cdot T1_{ss} - WT1}{G12} \quad \text{Equation 3-88}$$

$$A = \frac{T1\phi - T1_{ss} - \frac{DER1}{m_2}}{1 - \frac{m_1}{m_2}} \quad \text{Equation 3-89}$$

$$B = \frac{DER1 - m_1 \cdot A}{m_2} \quad \text{Equation 3-90}$$

$$AA = \frac{A}{G12} (G1 + C1 \cdot m_1) \quad \text{Equation 3-91}$$

$$BB = \frac{B}{G12} (G1 + C1 \cdot m_2) \quad \text{Equation 3-92}$$

The temperature is then

$$T1 = Ae^{m_1 t} + Be^{m_2 t} + T1_{ss} \quad \text{Equation 3-93}$$

$$T2 = AAe^{m_1 t} + BB e^{m_2 t} + T2_{ss} \quad \text{Equation 3-94}$$

3.2 Analysis of the Depth to which the Heat diffuses in a given Time

The analysis of the short time negative sequence event assumed that the time was short enough that the heat was stored in the volume of current penetration. In this case we were considering a fraction of a second. This assumption was verified by finite element analysis. In certain cases we may be interested in events which take longer. This could be a high impedance fault (lower current) that is not interrupted for many seconds for example. We may also be interested in motoring events that could go on for minutes. In these cases the thermal model should be modified to account for the heat being transferred from the surface into the body of the rotor. While this is more complex, we can make an estimate as to how deep the heating goes in a given time. We make use of closed form solutions of the heat equation or diffusion equation in a one dimensional or semi-infinite solid.²

The analysis is given in the reference and only the pertinent result is included here. The idea is that we have a large solid body at a uniform temperature. We then apply a step function of temperature (changing the boundary temperature) and look at the penetration of heat into the body. The definition of a depth is subject to judgment since even at $t = 0^+$ there is a change of temperature, perhaps very small, at great distances from the surface. Let us take as a working definition, the distance at which the temperature change is greater than 5% of the difference between the initial temperature and the applied temperature. This is illustrated using the equivalent ladder network circuit shown below in Figure 3-13.

The nodes are at initial temperature T_I when the applied boundary temperature T_{AP} is connected to node 1 by closing the switch. We would like to establish a two node equivalent circuit that accounts for the increasing heat penetration.

The graph Figure 3-15 shows the nodal temperatures in the first few nodes of the circuit as a function of time.

² Fishenden and Saunders, "Introduction to Heat Transfer"

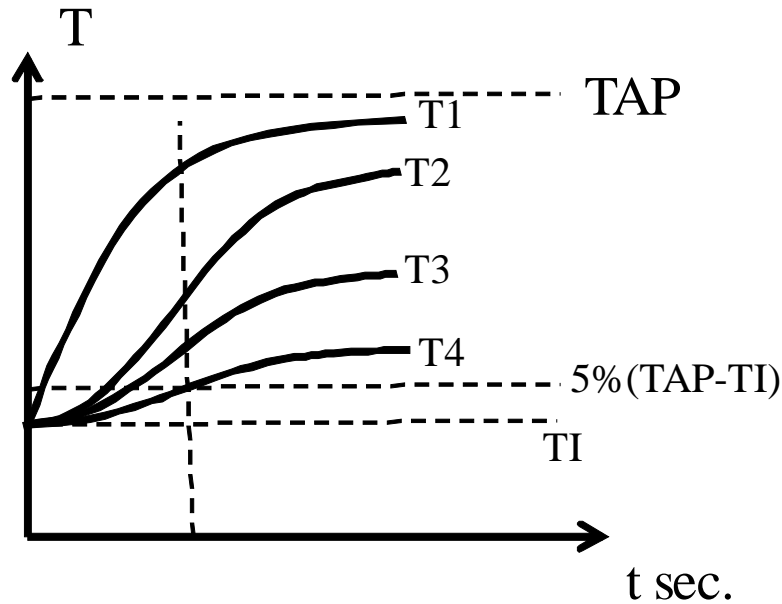


Figure 3-15
Transient temperature at different depths

Using our criterion that the temperature rise is at least 5% of the total temperature difference between the initial and final temperatures we see that at a given time, node 4 is at the effective depth. Below that depth, the temperature rise is lower than the 5% cut-off and therefore not much heat has penetrated.

The graph of Figure 3-16 shows the coefficient R_a versus the per unit temperature difference T_{ef} .

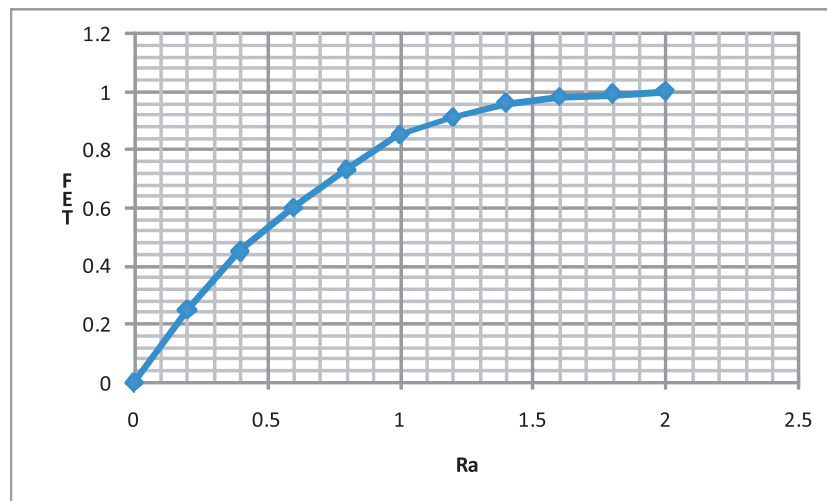


Figure 3-16
Evaluation of coefficient R_a

We define

$$T_{ef} = \frac{TAP - T(n)}{TAP - TI} \quad \text{Equation 3-95}$$

and

$$Ra = \frac{x}{2\sqrt{\frac{k}{c_v}t}} \quad \text{Equation 3-96}$$

where

k = thermal conductivity (Watt/ $^{\circ}C - in$)

c_v = volumetric specific heat (Watt-sec/in³)

t = seconds

To determine the distance x_l at time t_l we use tequations 97 and 98.:

$$\frac{x_l}{2\sqrt{\frac{k}{c_v}t}} = \frac{TAP - T_l}{TAP - TI} = 0.95 \quad \text{Equation 3-97}$$

$$x_l = 1.9\sqrt{\frac{k}{c_v}t_l} \quad \text{Equation 3-98}$$

3.3 Retaining Ring

The retaining ring model takes the current from the straight part of the machine. I_{ps0} is the currents that enters the retaining ring. The Amperes per inch entering the ring is

$$I_{pz} = \frac{I_{spo}}{T_{rsp}} \quad \text{Equation 3-99}$$

$$I_{zf}(\theta) = I_{pz} \cos \frac{\pi p}{2T_{pph}} \quad \text{Equation 3-100}$$

$$I_{zf}(z) = I_{pz} \cos \frac{\pi Z}{2L_{rrt}} \quad \text{Equation 3-101}$$

$$I_{pf}(z) = I_{pp} \sin \frac{\pi Z}{2L_{rrt}} \quad \text{Equation 3-102}$$

There is a relationship between the peripheral and axial current in the retaining ring. Since

$$\int_0^{T_{pph}} I_{pz} \cos \frac{\pi p}{2T_{pph}} \cdot dp = \int_0^{L_{rrt}} I_{pp} \sin \frac{\pi Z}{2L_{rrt}} \cdot dz \quad \text{Equation 3-103}$$

$$I_{pp} = I_{pz} \cdot \frac{T_{pph}}{L_{rrt}} \quad \text{Equation 3-104}$$

The losses produced by these sinusoidal current distributions are found as follows: Referring to Figure 3-17.

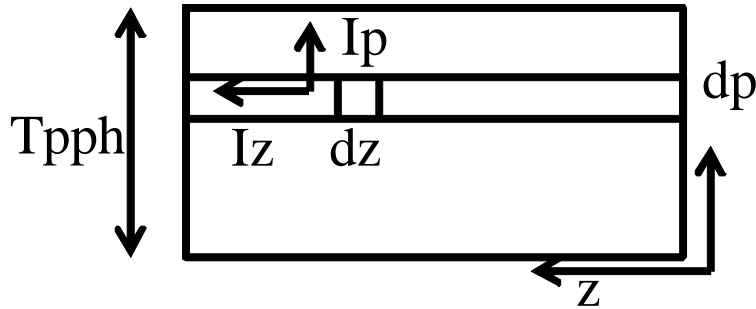


Figure 3-17
Expanded view of retaining ring

The resistance are found as

$$R_p = \frac{\rho \Delta p}{\Delta z \Delta r} \quad \text{Equation 3-105}$$

$$R_z = \frac{\rho \Delta z}{\Delta \rho \Delta r} \quad \text{Equation 3-106}$$

$$\Delta r = \delta \quad \text{Equation 3-107}$$

For a strip (figure 3-17), the losses from I_z are given as

$$L_{rz} = \frac{\rho}{\Delta r} \int_0^{L_{rrt}} i_z^2 dz \quad \text{Equation 3-108}$$

the losses are from I_p are given as

$$L_{rp} = \frac{\rho}{\Delta r} \int_0^{L_{rrt}} i_p^2 dz \quad \text{Equation 3-109}$$

Now

$$I_{pz}(z) = I_{pp} \sin \frac{\pi z}{2 L_{rrt}} \quad \text{Equation 3-110}$$

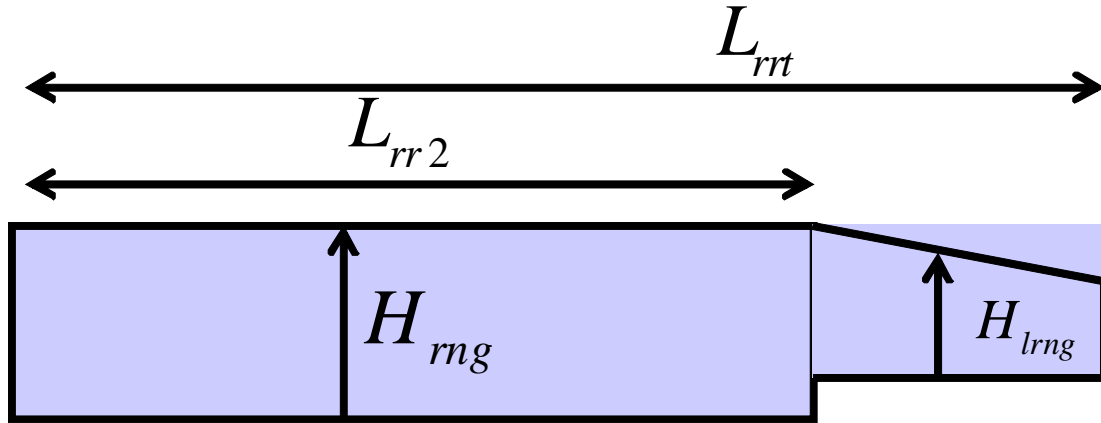


Figure 3-19
Retaining ring dimensions

To find the surface resistances we use the same formulation as the weges. These are formed from the heat transfer coefficient times the surface area as given in equations 3-117 and 3-118.

$$R_{s1} = \frac{1}{h_{str} L_{rr1}} \quad \text{Equation 3-117}$$

$$R_{s2} = \frac{1}{h_{str} L_{rr2}} \quad \text{Equation 3-118}$$

The thermal resistances of the body are given in equations 3-119-3-123

$$R_{r1} = \frac{\rho_{trr} \cdot \frac{H_{lrng}}{2}}{L_{rr1}} \quad \text{Equation 3-119}$$

$$R_{r2} = \frac{\rho_{trr} \cdot \frac{H_{lrng}}{2}}{L_{rr2}} \quad \text{Equation 3-120}$$

$$R_{x12} = \rho_{trr} \left(\frac{L_{rr1}}{2 \cdot H_{lrng}} + \frac{L_{rr2}}{2 \cdot H_{lrng}} \right) \quad \text{Equation 3-121}$$

$$R_{bd} = R_{s2} + R_{r2} \quad \text{Equation 3-122}$$

$$R_{LP} = R_{s1} + R_{r1} \quad \text{Equation 3-123}$$

The thermal capacitances are

$$C_{r1} = c_{vrr} H_{lrng} L_{rr1} \quad \text{Equation 3-124}$$

$$C_{r2} = c_{vrr} H_{lrng} L_{rr2} \quad \text{Equation 3-125}$$

$$W_{r1} = \frac{L_{rr1}}{L_{rrt}} W_{pst} \quad \text{Equation 3-126}$$

$$W_{r2} = W_{pst} - W_{r1} \quad \text{Equation 3-127}$$

3.4 Model for the Flex Slot Region Based on Electric Conduction

The flexibility slot region is one of the locations on the rotor which may be subjected to damage since the negative sequence eddy currents crowd around the ends of the slots, increasing the current density near the first rotor slot. There has been damage noted in this region as described in the previous report. We see in Figure 3-20 below the cross section of the flex slot. This is normally cut with a circular saw and therefore has a circular shape.

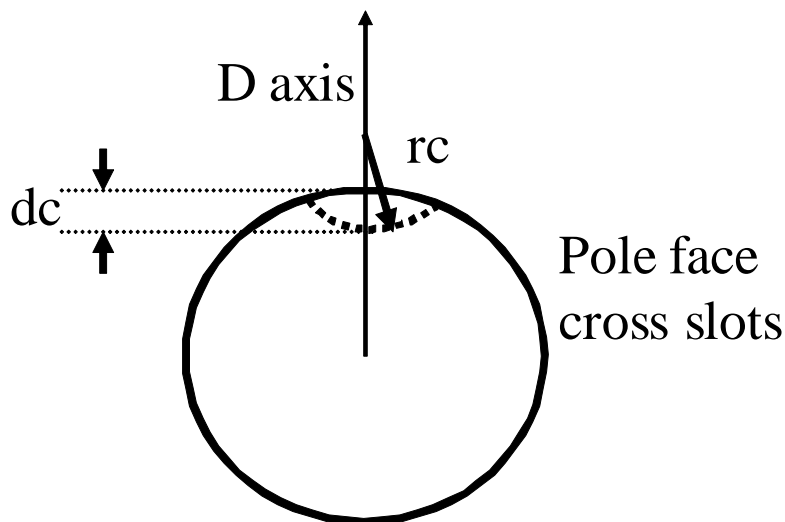


Figure 3-20
Pole face cross slots

As the axial currents come down the rotor length they must either go beneath the cross slot, which means a longer path length and higher impedance, or go around the slot and crowd into the region near the first rotor wedge. This is shown in the figure below (Figure 3-21). The current division is complex but can be approximated by the equivalent circuit of figure.

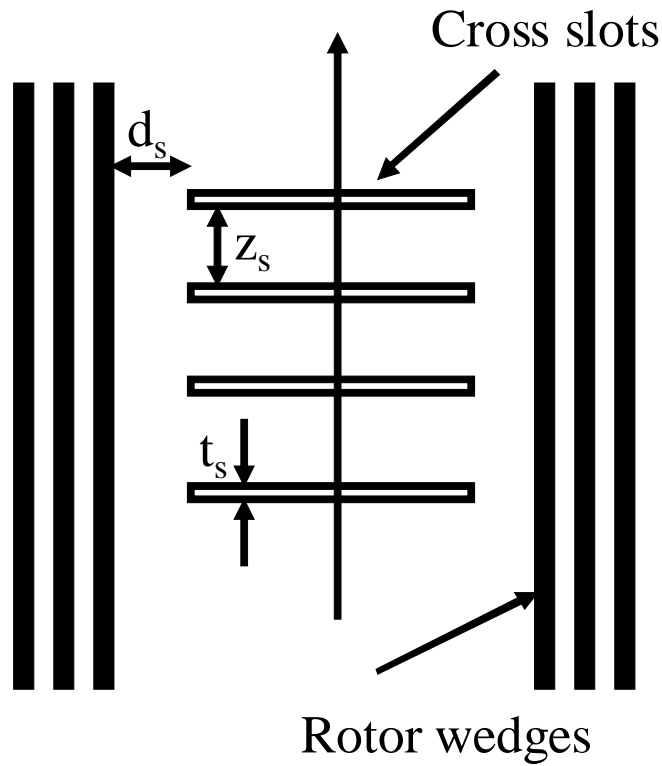


Figure 3-21
Rotor wedges

Figure 3-22 illustrates the conduction (resistance) network. The sum of the currents around the three nodes are,

$$I_1 = V_1(G_{1g} + G_{2g}) - V_2G_{12} \quad \text{Equation 3-128}$$

$$I_2 = -V_1G_{12} + V_2(G_{12} + G_{23} + G_{2g}) - V_3G_{23} \quad \text{Equation 3-129}$$

$$I_3 = -V_2G_{23} + V_3(G_{23} + G_{3g}) \quad \text{Equation 3-130}$$

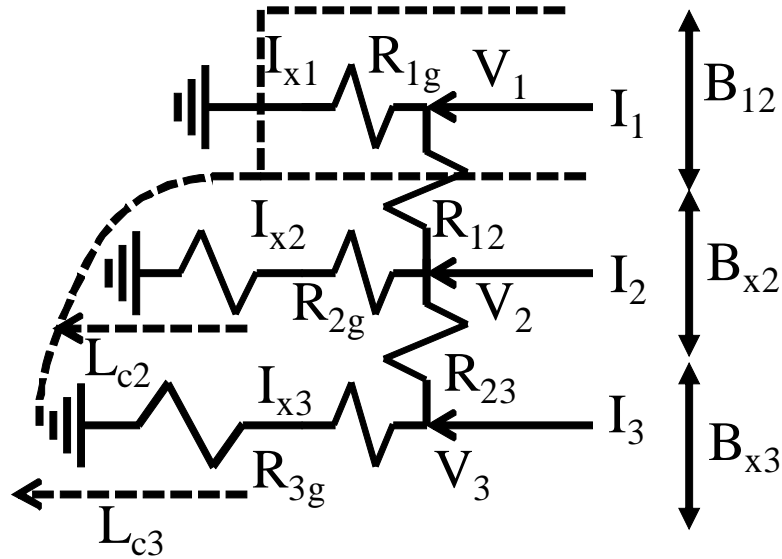


Figure 3-22
Conduction (resistance) network

We solve these by back substitution for the nodal voltages as shown below

For the conductance we define

$$G_{1t} = G_{1g} + G_{12} \quad \text{Equation 3-131}$$

$$G_{2t} = G_{12} + G_{23} + G_{2g} \quad \text{Equation 3-132}$$

$$G_{3t} = G_{23} + G_{3g} \quad \text{Equation 3-133}$$

The current is

$$I_{tot} + I_2 + \left(G_{12} \frac{I_1}{G_{1t}} \right) + \left(G_{23} \frac{I_3}{G_{3t}} \right) \quad \text{Equation 3-134}$$

$$G_{tot} = G_{2t} - \frac{G_{12}^2}{G_{1t}} - \frac{G_{23}^2}{G_{3t}} \quad \text{Equation 3-135}$$

$$V_2 = \frac{I_{tot}}{G_{tot}} \quad \text{Equation 3-136}$$

$$I_{x2} = V_2 \cdot G_2 \quad \text{Equation 3-137}$$

$$V_1 = \frac{I_3 + V_2 \cdot G_{23}}{G_{1t}} \quad \text{Equation 3-138}$$

$$I_{x1} = V_1 \cdot G_{1g} \quad \text{Equation 3-139}$$

$$V_3 = \frac{(I_1 + V_2 \cdot G_{12})}{G_{1t}} \quad \text{Equation 3-140}$$

$$I_{x3} = V_3 \cdot G_{3g} \quad \text{Equation 3-141}$$

The resistances in this case are all nonlinear (see following section on nonlinear depth of penetration). The currents I_1 , I_2 , and I_3 are assumed uniform (amps/inch) and are found from I_{spp} in the same way that the slot currents are found. The strategy is as follows.

We first establish I_1 , I_2 , and I_3 from I_{spp} . These are given in equations 3-142 – 3-144.

$$I_1 = \frac{B_{x1}}{T_{rsp}} \cdot I_{spp} \quad \text{Equation 3-142}$$

$$I_2 = \frac{B_{x2}}{T_{rsp}} \cdot I_{spp} \quad \text{Equation 3-143}$$

$$I_3 = \frac{B_{x3}}{T_{rsp}} \cdot I_{spp} \quad \text{Equation 3-144}$$

We now estimate the first iteration values of I_1 , I_2 , and I_3 .

$$I_{x10} = I_1 \quad \text{Equation 3-145}$$

$$I_{x20} = I_2 \quad \text{Equation 3-146}$$

$$I_{x30} = I_3 \quad \text{Equation 3-147}$$

$$K_{r0} = 5640 \sqrt{\rho_i B_s f} \quad \text{Equation 3-148}$$

Now find the depth of penetration and the effective resistance of each path. A sequence of calculation is now given in equations 3-149-3-164. If the solution is not converged we return to (A). If we have reached convergence we continue.

(A)

$$Hp_1 = \frac{\sqrt{2} I_{x10}}{B_{x1}} \quad \text{Equation 3-149}$$

$$\delta_1 = K_{ro} \left(\frac{Hp_1}{B_{x1}} \right)^2 \quad \text{Equation 3-150}$$

$$R_{1g} = \rho_i \frac{L_{fjh} / 2}{\delta_1 B_{x1}} \quad \text{Equation 3-151}$$

$$Hp_2 = \frac{\sqrt{2} I_{x20}}{B_{x2}} \quad \text{Equation 3-152}$$

$$\delta_2 = K_{r0} (H_{p2})^{\frac{3}{2}} \quad \text{Equation 3-153}$$

$$R_{2g} = \rho_i \frac{L_{fxh} / 2 + L_{c2}}{\delta_2 B_{x2}} \quad \text{Equation 3-154}$$

$$Hp_3 = \frac{\sqrt{2} I_{x30}}{B_{x3}} \quad \text{Equation 3-155}$$

$$\delta_3 = K_{r0} (H_{p3})^{\frac{3}{2}} \quad \text{Equation 3-156}$$

$$R_{3g} = \rho_i \frac{L_{fxh} / 2 + L_{c3}}{\delta_3 B_{x3}} \quad \text{Equation 3-157}$$

$$R_{12} = \rho_i \left(\frac{B_{x1}}{\delta_i L_{fxh}} + \frac{B_{x2}}{\delta_2 (L_{fxh} + L_{c2} / 2)} \right) \quad \text{Equation 3-158}$$

$$R_{23} = \rho_i \left(\frac{B_{x2}}{\delta_2 (L_{fxh} + L_{c2} / 2)} + \frac{B_{x3}}{\delta_3 (L_{fxh} + L_{c3} / 2)} \right) \quad \text{Equation 3-159}$$

$$G_{1g} = \frac{1}{R_{1g}} \quad \text{Equation 3-160}$$

$$G_{2g} = \frac{1}{R_{2g}} \quad \text{Equation 3-161}$$

$$G_{3g} = \frac{1}{R_{3g}} \quad \text{Equation 3-162}$$

$$G_{12} = \frac{1}{R_{12}} \quad \text{Equation 3-163}$$

$$G_{13} = \frac{1}{R_{23}} \quad \text{Equation 3-164}$$

Solve for the currents and voltages in the network and compare them to the last values of the currents and voltages. If the differences of values are below a given level then stop. If not, change the currents and go to (A) and repeat as necessary

From the solution the loss per unit area of surface is

$$W_{psi} = 1.51 \times 10^{-4} \sqrt{\rho_i \cdot B_s \cdot f \cdot H^3_{p1}} \quad \text{Equation 3-165}$$

$$W_x = W_{psi} \cdot B_{x1} \cdot L_{x1} \quad \text{Equation 3-166}$$

3.4.1 Temperature of the Flex Slot

We obtain the depth δ_i from the current I_{x1} . For the other parameters we use

$$C_1 = N\delta_i L_{x1} B_{x1} c_{vi} \quad \text{Equation 3-167}$$

$$C_2 = \delta_i L_{x1} B_{x1} c_{vi} \quad \text{Equation 3-168}$$

c_{vi} = specific heat (volume)

For the temperature T_2 (near the surface), we have

$$T_2 = Ae^{m1t} + Be^{m2t} + T_{2\text{steady state}} \quad \text{Equation 3-169}$$

In this model

$$N = 3 \quad \text{Equation 3-170}$$

$$Q = (\text{see below}) \quad \text{Equation 3-171}$$

$$L_{x1} = \text{BSLH (half slot)} \quad \text{Equation 3-172}$$

$$L_{x2} = 3 \cdot L_{x1} \quad \text{Equation 3-173}$$

$$T_{i1} = T_{i2} = T_p = T_i \quad \text{Equation 3-174}$$

The thermal surface resistance is as before the inverse of the heat transfer coefficient times the surface area

$$R_s = \frac{1}{h_{st} \cdot L_{x1} \cdot B_{x1}} \quad \text{Equation 3-175}$$

The body resistances are

$$R_{i3} = \frac{\rho_{ii} \cdot \frac{\delta_i}{2}}{L_{x1} \cdot B_{x1}} \quad \text{Equation 3-176}$$

$$R_{i4} = \frac{\rho_{ii} \cdot \left(\frac{\delta_i}{2} + N \frac{\delta_i}{2} \right)}{L_{x1} \cdot B_{x1}} \quad \text{Equation 3-177}$$

$$R_{i5} = \frac{\rho_{ii} \cdot \left(N \frac{\delta_i}{2} + Q\delta_i \right)}{L_{x1} \cdot B_{x1}} \quad \text{Equation 3-178}$$

$$R_{i1} = \frac{\rho_{ii} \cdot \frac{1}{2} (L_{x1} + L_{x2})}{B_{x1} \cdot Q \cdot \delta_1} \quad \text{Equation 3-179}$$

$$R_{i2} = \frac{\rho_{ti} \cdot \frac{1}{2}(L_{x1} + L_{x2})}{B_{x1} \cdot N \cdot \delta_1} \quad \text{Equation 3-180}$$

Now combine

$$R_{is} = R_s + R_{i3} \quad \text{Equation 3-181}$$

Now to find Q we use the following process. First for a given time T_L we have

$$X_L = 1.9 \sqrt{\frac{k}{c_v} T_L} \quad \text{Equation 3-182}$$

$$D_{LH} = \frac{1}{2}(X_L - 1.5\delta_1) \quad \text{Equation 3-183}$$

$$Q = \frac{D_{HL}}{\delta_1} \quad \text{Equation 3-184}$$

To find B_{ma} we use the following process.

$$R_{am} = \frac{1.5\delta_1 + Q\delta_1}{2 \sqrt{\frac{k}{c_v} T_L}} \quad \text{Equation 3-185}$$

$$R_{A1} = \frac{1.5\delta_1}{2 \sqrt{\frac{k}{c_v} T_L}} \quad \text{Equation 3-186}$$

$$B_{ma} = \frac{1 - R_{am}}{1 - R_{A1}} \quad \text{Equation 3-187}$$

$$B_{xo} = 1.0 - 0.5B_{ma} \quad \text{Equation 3-188}$$

To apply the model we use T_g as the air gap temperature. T_p , T_p as the tooth temperature. T_{10} , T_{20} are the initial temperatures at $t = 0$. W_x is the loss (current injection into the model). This is injected at node 2 in Figure 3-24 while at node 1 there is no injection.

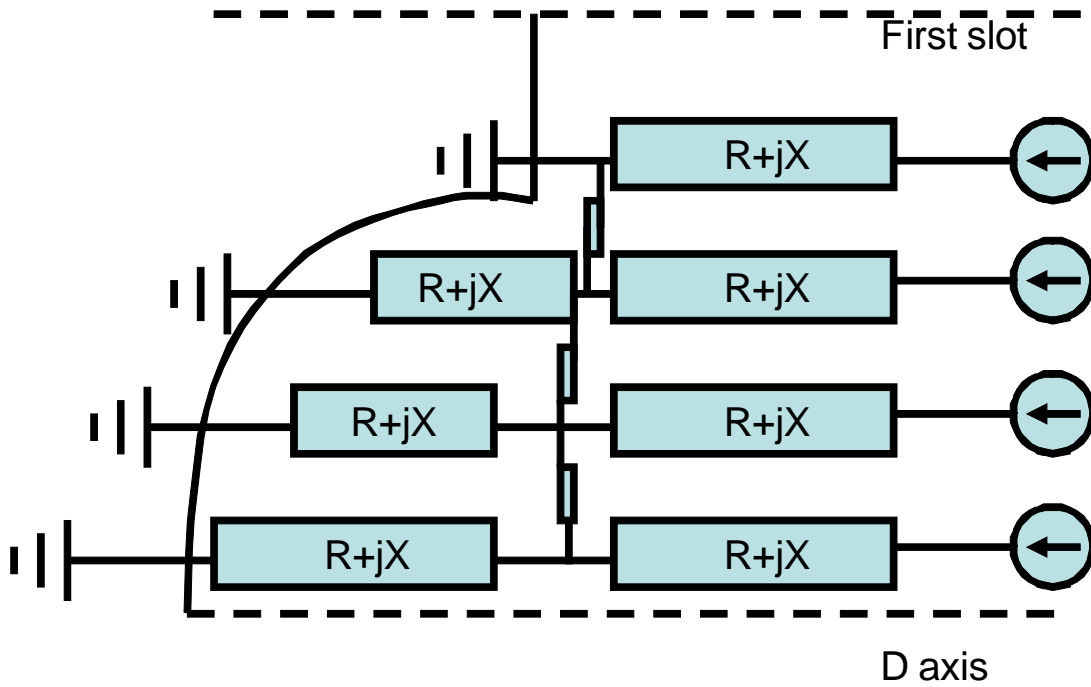


Figure 3-23
Electrical network for the flex slot

$$G_{1c} = \frac{B_{x0}}{R_{i5}} \quad \text{Equation 3-189}$$

$$G_{2d} = \frac{1.0}{R_{is}} \quad \text{Equation 3-190}$$

$$G_{1a} = \frac{1.0}{R_{i1}} \quad \text{Equation 3-191}$$

$$G_{2b} = \frac{1.0}{R_{i2}} \quad \text{Equation 3-192}$$

$$G_{12} = \frac{1.0}{R_{i4}} \quad \text{Equation 3-193}$$

$$T_{bc} = T_p = T_i \quad \text{Equation 3-194}$$

$$T_{bd} = T_g \quad \text{Equation 3-195}$$

$$T_{ba} = T_{i1} \quad \text{Equation 3-196}$$

$$T_{bb} = T_{i2} \quad \text{Equation 3-197}$$

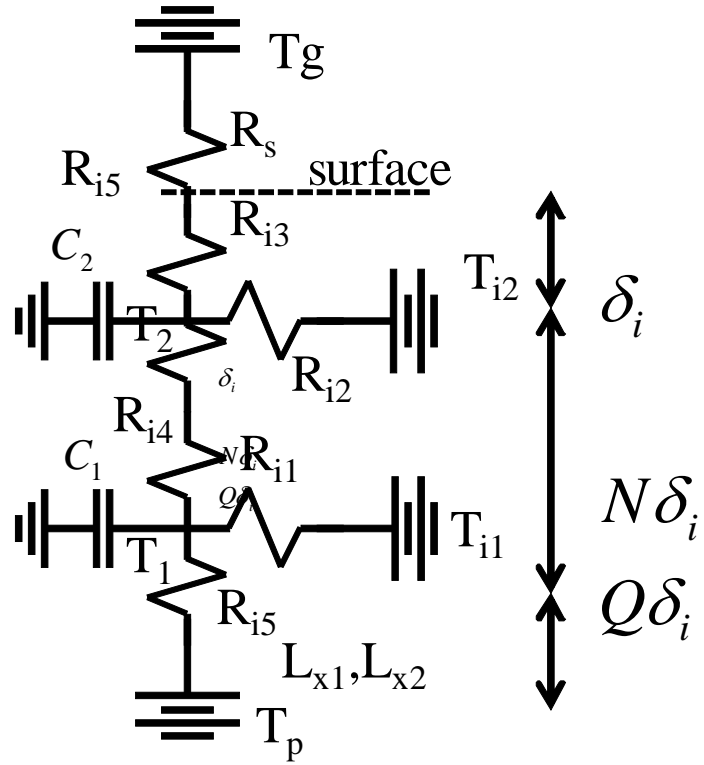


Figure 3-24
Temperature model for the flex slot

4

APPLYING THE SIMPLIFIED MODELS TO MOTORING

There are a number of issues in applying the simplified models to the case of motoring. As far as the physics of the situation is concerned, the problem is essentially the same. There are some issues to consider however and these have to do with the assumptions that were used in coming up with the simplified models. In both cases we have the stator MMF in relative motion with the rotor and induced currents in the rotor will cause heating. The frequency and time duration may be very different and we should look carefully at these to determine if the assumptions are still valid. We can envision two different cases of motoring operation as extreme limits. In the first case let us assume that the generator is at standstill or very low speed, for example on turning gear. If the machine is now accidentally connected to the system due to operator error or a malfunction of the breaker, the rotor is subjected to rated frequency eddy currents (or near rated frequency if the speed is not zero). In this case the skin depth is still rather small and the currents are very close to the surface of the rotor. The skin depth is generally smaller than the depth of the wedge, and the field winding is not involved being too deep in the rotor. In this case the simplified models should still be valid for short times. The frequency must be changed to reflect the rated frequency minus the rotational frequency assuming that all three phases are involved (balanced assumption). If, for example, the machine is at standstill and a single phase is energized, then we have the situation in which we have both positive and negative sequence currents. At standstill these would each look like rated frequency currents on the rotor surface. As the machine accelerated, which it would do if it were on turning gear when the connection was made. The frequency of positive sequence component of eddy current would decrease and the negative sequence component would increase. These effects can be handled by the model by changing the frequency which is an independent input to the model. The unknown in this case is that due to the low speed of the rotor, the contact resistances will likely be different. The shrink fit of the retaining ring on the pole face and teeth will be greater and this should reduce the resistance. The contact of the retaining ring with the wedge will be less and this resistance will be higher and perhaps significantly higher. The wedge segments in the slot will also be looser and the transfer of the current from wedge segment to wedge segment will be affected as will the transfer of the current between wedge and tooth. This is an unknown effect and there is quite likely great variability from machine to machine and even from slot to slot in the same machine. With these exceptions, the models should be valid for the losses and temperatures for short time periods in which most of the heat is stored in the thermal mass of the machine. The second case of motoring (or possibly induction generating) occurs when the machine is near synchronous speed. One possibility is that the machine is operating normally when there is a loss of excitation. In this case the machine will lose synchronism and due to the droop characteristic of the governor will accelerate above synchronous speed. This is illustrated in Figure 4-1.

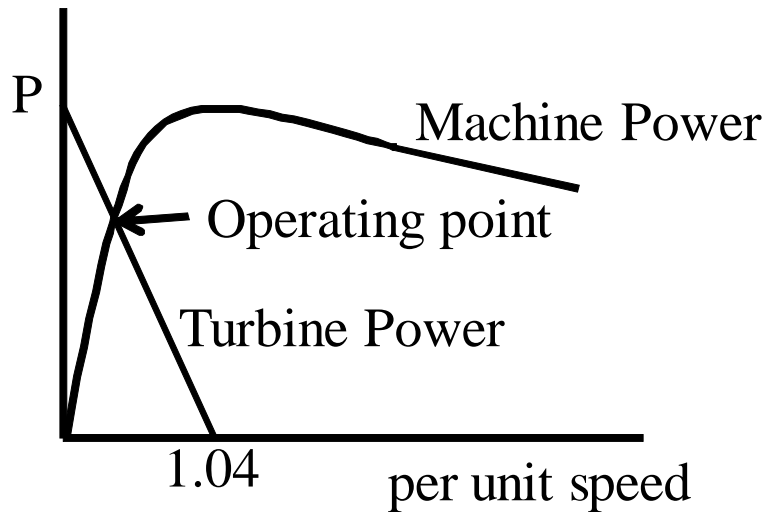


Figure 4-1
Generator and governor steady state characteristic

The machine above synchronous speed will operate as an induction generator and deliver real power to the system at rated frequency while drawing a large magnetizing current from the system. The governor will compensate for the overspeed by reducing the mechanical power of the shaft. The steady state relationship between speed and power is linear and the power goes to zero typically when the speed increases by a few per cent over synchronous speed. This is the droop characteristic and a number like 4% is typical. The machine in this case is operating at a few per cent slip at super-synchronous speed. The frequency of the induced current in the rotor is a few hertz at most. The skin depth on the rotor is large. In this case the currents penetrate much further than in the negative sequence case. The assumptions we have used are not entirely valid. For example, the field winding may share a large portion of the current. The situation is much less dangerous than the negative sequence fault since the larger skin depth means that the

effective rotor resistance is smaller $\left(R \sim \frac{1}{\sqrt{\delta}} \right)$ Which means that the losses are much lower

for an equivalent current. We also have the thermal mass proportional to the skin depth so that for a given energy input the temperature rise is much lower. The problems usually develop in these cases if the asynchronous operation lasts a long time - several minutes to 10's of minutes. In these rare cases wedges have melted and come out of the slot. The thermal assumptions used in the negative sequence models also must be considered. For short incidents (a few seconds) these should be generally valid. If the incident lasts minutes or longer however, there is sufficient time for the heat to transfer both into the rotor body or into the air gap. The models included here do have these capabilities but not enough resolution to give an accurate temperature distribution.

5

SUMMARY AND CONCLUSIONS

This is part 2 of a study that provides a method of quick assessment of turbine generator rotors following an negative sequence event. The method is primarily for the determination of hot spot temperatures in the rotor Mechanical stress due to thermal expansion and the potential for arcing have also been studied (see Reference 1). It was concluded that thermal stress was not likely to be dangerous and that arcing damage, while potentially very serious, would require further research. In the thermal model introduced in part 1 and documented in this report, we invoke equivalent circuits for the eddy currents, losses and temperature. The methods are most accurate for faults with short durations, where thermal convection to the a or gap and conduction deep into the rotor have not had much time to significantly affect the results. Where possible, these simplified models have been verified with the finite element method.

The models take as their input, the negative sequence current and duration of the event. The electromagnetic circuit takes into account the skin depth, self and mutual coupling, resistance and saturation in the steel parts. In the case of nonlinear effects, the circuits must be solved by iterative methods. The currents found in the electromagnetic models then yield the losses and these are input for the thermal circuits. These give the temperature versus time at various sensitive locations in the rotor.

We have presented models for the following:

In the wedge region we have two cases: the sunken wedge and the flush wege geometries. In both cases the effects of the field winding are ignored.

In the pole face region we have only the nonlinear steel to represent.

In the flex slot region we model the currents near the end of the cross- slot as an electrical network and can account for the crowding of the currents toward the first slot.

In the retaining ring area we have models for the shring fit region and the retaining ring body region.

It is possible to use these models for the case of motoring. The applicability will depend on the nature of the event. If the machine is energized at or near standstill, the methods should still be useful. If the motoring occurs near rated speed, the models are less applicable.

The study would benefit if we had the test results from one of the manufacturers with geometry to check the electrical and thermal behavior.

A

EDDY CURRENTS IN STEEL³

We have seen in the one dimensional case that

$$\frac{\partial^2 B_x}{\partial x^2} = \mu\sigma \frac{\partial B_x}{\partial t} \quad \text{Equation A-1}$$

and the flux density at any depth can be found as

$$B_x = \text{Re} \left\{ B_0 e^{(j\omega t - x\sqrt{j\omega\mu\sigma})} \right\} \quad \text{Equation A-2}$$

where B_0 is the flux density at the surface. The total flux is then

$$\psi_m(t) = \int_0^\infty B_x dx = \frac{B_0}{\sqrt{j\omega\mu\sigma}} e^{j\omega t} \quad \text{Equation A-3}$$

In terms of the total flux, the flux density can be written

$$B_x = \text{Re} \left\{ \sqrt{j\omega\mu\sigma} \psi_{m\max} e^{(j\omega t - x\sqrt{j\omega\mu\sigma})} \right\} \quad \text{Equation A-4}$$

Now let us consider a nonlinear material characteristic as shown in Figure A-1.

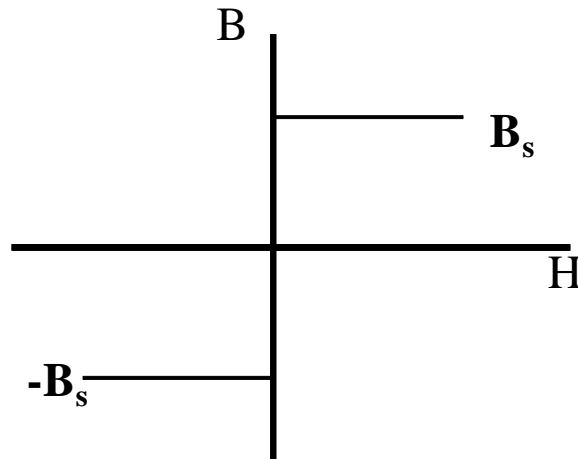


Figure A-1
Limiting B-H curve of steel

³ H. M. McConel, "Eddy Current Phenomena in Ferromagnetic Material", AIEE, July 1954, pp. 226-233.

The flux density has only two states $\pm B_s$, the saturation flux density. The material can switch only when $H = 0$. A sinusoidal flux, $\psi_m(t) = \text{Re}\{\psi_m e^{j\omega t}\}$ can be supported in a material like this by a series of square or rectangular waves.

Since $\psi_m(t)$ is periodic, we can construct it from square waves of the same period. This is illustrated in Figure A-2. This leaves two possibilities for the magnetized iron. It is magnetized $\pm B_s$ periodically at a frequency ω , or it is constant at $\pm B_s$ being left at that state from a previous excitation.

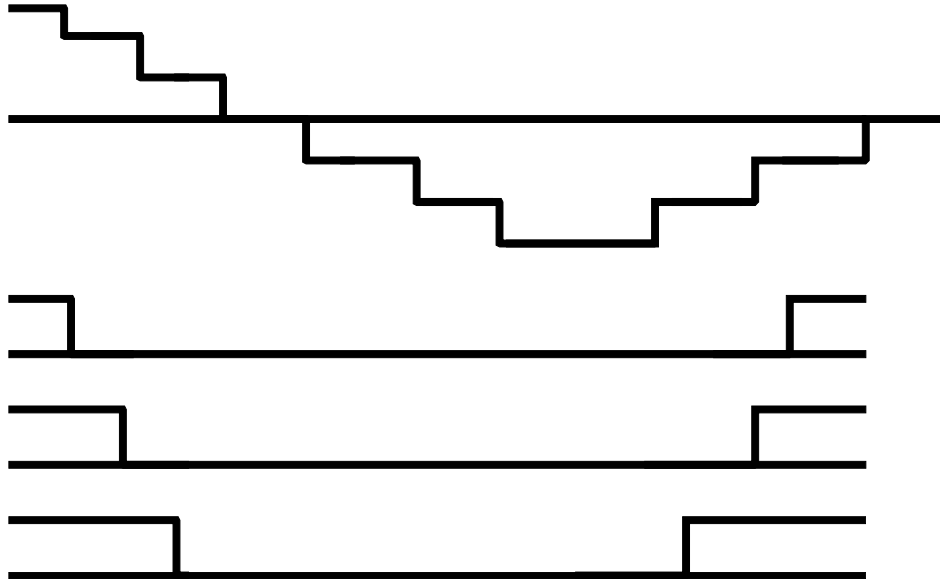


Figure A-2
Making A sinusoidal wave from square waves

At some instant of time the material above a certain level x_1 is magnetized to $-B_s$, below this level it is $+B_s$. At some time later this layer of separation has moved to x_2 . The movement of the surface took place in a time Δt . The phase shift between the rectangular waves at z_1 and z_2 is $\omega\Delta t$ radians. The surface of separation will move to a certain depth and no further. At this depth the total flux above the surface of separation is $-\psi_{m_{max}}$. If we call this depth δ , then

$$\delta = \frac{\psi_{m_{max}}}{B_s} \tag{Equation A-5}$$

We note several things. First, the depth of penetration δ , is interpreted differently than in the linear case. In the linear case, the depth of penetration is that depth at which the flux density is $1/e$ of its value at the surface. The depth of penetration depends only on the frequency and the material properties (conductivity and permeability) In the nonlinear limiting case the depth of penetration is the maximum distance at which the material switches from $+B_s$ to $-B_s$. This distance depends on the total flux and the saturation flux density B_s . The surface of separation has moved from $x = 0$ to $x = \delta$ in one half cycle since the flux has changed from $\psi_{m_{max}}$ to $-\psi_{m_{max}}$. This means that the phase shift between the rectangular waves at $x = 0$ and $x = \delta$ is π radians.

Consider now that the surface of separation is at location x' . As the surface moves from x' to $x' + \Delta x'$, the change in flux is

$$\Delta\psi_m = -2B_s\Delta x' \quad \text{Equation A-6}$$

In differential form we have

$$\frac{dz'}{d\psi_m} = -\frac{1}{2B_s} \quad \text{Equation A-7}$$

We can integrate this equation starting from $\psi_{m_{max}}$ and $x = 0$

$$z' = \frac{1}{2B_s} \int_{\psi_{m_{max}}}^{\psi_m} -d\psi \quad \text{Equation A-8}$$

So that

$$z' = \frac{\psi_{m_{max}} - \psi_m(t)}{2B_s} \quad \text{Equation A-9}$$

With this model we can find the eddy current distribution as

$$J = \sigma E \quad \text{Equation A-10}$$

Where the electric field is found as

$$\nabla \times E = -\frac{\partial B}{\partial t} \quad \text{Equation A-11}$$

In integral form this becomes

$$\oint_C E \cdot dl = -\frac{\partial}{\partial t} \iint_S B \cdot dS \quad \text{Equation A-12}$$

Where the curve C bounds the surface S. If the curve C encloses a region which does not contain the surface of separation between $+B_s$ and $-B_s$ then the integral will be zero. That is to say, the flux density in the region is constant. IF however the contour intersects the surface of separation then there will be an induced electric field which will depend on the velocity at this surface. For this one dimensional case we can evaluate the integral directly. Consider Figure A-3.

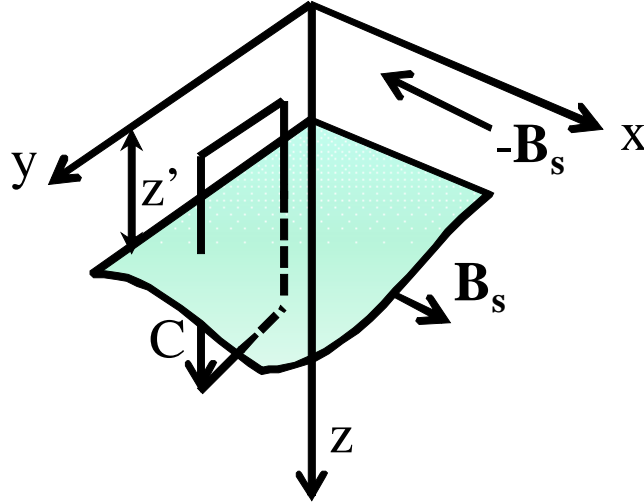


Figure A-3
Separation surface and coordinate system

The flux density has only an x component. We choose the integration path to be a closed contour in the yz plane. At some instant the surface of separation is at a depth z' and is moving in the z direction. The intersection of the line integral and the surface of separation is a line segment of length Δy . The electric field, E , has only a y component. It is constant above the surface of separation and below the surface of separation, with a discontinuity at the surface. At some time t , the velocity of the surface is $\frac{\partial z'}{\partial t}$ and the area with $-B_x$ is S_2 , where $S_1 + S_2 = S$. At some later

time $t + \Delta t$, the surface has moved a distance $\frac{\partial z'}{\partial t} \Delta t$ and an area of $-B_x$ is $S_1 + \frac{\partial z'}{\partial t} \Delta t \Delta y$ and the area with $+B_x$ is $S_2 - \frac{\partial z'}{\partial t} \Delta t \Delta y$. The integral can then be written as

$$E_y / z' - \Delta z' \Delta y - E_y / z' + \Delta z' \Delta y = \frac{2B_s \frac{\partial z'}{\partial t} \Delta t \Delta y}{\Delta t} \quad \text{Equation A-13}$$

so that

$$E_y / z' - \Delta z' - E_y / z' + \Delta z' = 2B_s \frac{\partial z'}{\partial t} \quad \text{Equation A-14}$$

which describes the discontinuity in the electric field at the surface of separation.

From a physical standpoint, the electric field below the surface of separation must be zero. If this were not true, uniform current would flow from the surface to infinity which would require an infinite amount of energy.

Therefore

$$E_y = 2B_s \frac{\partial z'}{\partial t}, (0 \leq z \leq z') \quad \text{Equation A-15}$$

and

$$E_y = 0, (z > z') \quad \text{Equation A-16}$$

During the next half cycle the sign of E will be reversed since the flux density will be changing from $-B_s$ to $+B_s$ but the velocity remains positive. In this model then, at any instant of time, the eddy current per unit depth is then

$$J = -2B_s \sigma z' \frac{\partial z'}{\partial t} \text{ Amps/unit depth} \quad \text{Equation A-17}$$

In terms of the applied sinusoidal flux

$$J = -2B_s \sigma \left(\frac{\psi_{m\max} - \psi_m(t)}{2B_s} \right) \left(-\frac{1}{2B_s} \frac{\partial \psi_m}{\partial t} \right) \quad \text{Equation A-18}$$

or

$$J = -\frac{\sigma}{2B_s} (\psi_{m\max} - \psi_m(t)) \frac{\partial \psi_m}{\partial t} \quad \text{Equation A-19}$$

$$\text{Using } \psi_m(t) = \psi_{m\max} \cos(\omega t) \quad \text{Equation A-20}$$

$$J = \frac{\omega \sigma}{2B_s} \psi_{m\max}^2 (1 - \cos(\omega t)) \sin(\omega t) \text{ Amperes/unit depth} \quad \text{Equation A-21}$$

As an example of the use of this model consider the currents carrying steel cylinder shown below in Figure A-4.

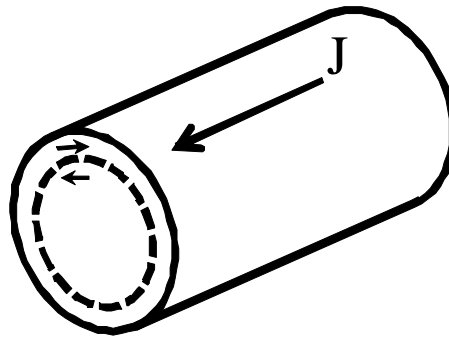


Figure A-4
Steel cylinder with axial current and skin depth

The separation boundary between the material magnetized $+B_s$ and $-B_s$ is located at $r = r'$. As the boundary moves it causes a change in flux linkage in the region $r < r'$. There is no change in the region $r' < r < R$. The flux linkage of a small element at time t is

$$\lambda(t) = -B_s(r' - r_s) + B_s(R - r') \text{ Wb/unit length} \quad \text{Equation A-22}$$

At time $t + \Delta t$ the surface of separation has moved to $r' + \Delta r'$ and the flux linkage has changed to

$$\lambda(t + \Delta t) = -B_s(r' + \Delta r' - r_s) + B_s(R - r' - \Delta r') \text{ Wb/unit length} \quad \text{Equation A-23}$$

The rate of change of flux linkage is therefore

$$\frac{d\lambda}{dt} = -2B_s \frac{dr'}{dt} \quad \text{Equation A-24}$$

This expression is independent of r_s so that every element in the region $0 < r < r'$ has the same induced electric field,

$$E_s = -2B_s \frac{dr'}{dt} \quad \text{Equation A-25}$$

The current density in the conducting annulus is

$$J = -2B_s \sigma \frac{dr'}{dt} \quad \text{Equation A-26}$$

and the total current in the conductor is

$$i = \pi(R^2 - r'^2)J \quad \text{Equation A-27}$$

or

$$i = -2B_s \pi \sigma (R^2 - r'^2) \frac{dr'}{dt} \quad \text{Equation A-28}$$

For the case in which i is sinusoidal taking the situation in the figure, the flux is increasing and the current i is positive. Integrating

$$-\int_R^{r'} 2\pi B_s \sigma (R^2 - r'^2) dr' = \int_0^t i dt \quad \text{Equation A-29}$$

$$\frac{2}{3} \pi B_s \sigma [r'^3 - R^2 r' + 2R^3] = \frac{I_{peak}}{\omega} (1 - \cos(\omega t)) \quad \text{Equation A-30}$$

If the current is not sufficient to cause the surface of separation to reach the center, i.e. $\delta < R$, we define the depth of penetration δ as

$$\delta = R - r'_{min} \quad \text{Equation A-31}$$

This gives

$$\frac{2}{3} \pi B_s \sigma \delta^2 (3R - \delta) = \frac{2I_{peak}}{\omega} \quad \text{Equation A-32}$$

If the depth of penetration is very small compared to the cylinder ($\delta \ll R$) then

$$\delta = \sqrt{\frac{I_{peak}}{\psi_m R B_s \omega \sigma}} \quad \text{Equation A-33}$$

In terms of the peak surface current density

$$J_{peak} = \frac{I_{peak}}{2\pi R} \quad \text{Equation A-34}$$

$$\delta = \sqrt{\frac{2J_{peak}}{\omega \sigma B_s}} \quad \text{Equation A-35}$$

If the current is such that the surface of separation just reaches the center of the cylinder at the end of each half cycle then $r' = 0$ and

$$I_{peak} = \frac{2}{3} \pi \omega \sigma B_s R^2 \quad \text{Equation A-36}$$

If the current is great enough that it reaches the center of the cylinder before the end of the half cycle, then for the rest of the cycle the conductor looks like a dc conductor with uniform current density throughout.

A.1 Losses

For the small depth of penetration case ($\delta \ll R$) the loss density (per unit volume) can be found as

$$P(t) = \frac{J^2}{\sigma} = \frac{i(t)^2}{\pi^2 (R^2 - r'^2)^2} \quad \text{Equation A-37}$$

and the loss per unit length is

$$P(t) = \frac{i(t)^2}{\pi \sigma (R^2 - r'^2)} \quad \text{Equation A-38}$$

The radius of the surface of separation, r' , is a function of time and for small δ

$$P(t) = \sqrt{\frac{B_s}{2\pi R\sigma}} \left(\frac{i(t)^2}{\sqrt{\int_0^t i(t) dt}} \right) \quad \text{Equation A-39}$$

Assuming that the current is sinusoidal,

$$P(t) = I_{peak}^2 \sqrt{\frac{B_s \omega}{2\pi R\sigma}} \left(\frac{\sin^2 \omega t}{\sqrt{1 - \cos \omega t}} \right) \quad \text{Equation A-40}$$

The average power over a half cycle is

$$P_{avg} = I_{peak}^2 \sqrt{\frac{B_s \omega}{2\pi R\sigma}} \int_0^\pi \frac{\sin^2 \theta}{\sqrt{1 - \cos \theta}} d\theta \quad \text{Equation A-41}$$

$$P_{avg} = I_{peak}^2 \sqrt{\frac{B_s \omega}{2\pi R\sigma}} \frac{4\sqrt{2}}{3\pi} \quad \text{Equation A-42}$$

In terms of the depth of penetration δ the loss in Watts per unit length is

$$P_{avg} = I_{peak}^2 \frac{8}{3\pi} \frac{1}{2\pi R\delta\sigma} \quad \text{Equation A-43}$$

If we now define the effective resistance of the cylinder as

$$R_{eff} = \frac{P_{avg}}{I_{RMS}^2} \quad \text{Equation A-44}$$

then

$$R_{eff} = \frac{16}{3\pi} \left(\frac{1}{2\pi R\delta\sigma} \right) \quad \text{Equation A-45}$$

Assume now that the applied field is sinusoidal. In this case

$$2B_s \sigma z' \frac{\partial z'}{\partial t} = J_{s\ peak} \sin(\omega t) \quad \text{Equation A-46}$$

The surface of separation is located at

$$z' = \sqrt{\frac{1}{B_s \sigma} \int_0^t J_{s\ peak} \sin(\omega t) dt} \quad \text{Equation A-47}$$

for each half cycle and the depth of penetration is

$$\delta = z_{max} = \sqrt{\frac{2J_{speak}}{B_s \omega \sigma}} \quad \text{Equation A-48}$$

In the conducting layer, the current density is

$$J = \frac{J_s}{z'} = \sqrt{B_s \omega \sigma J_{speak}} \frac{\sin \omega t}{\sqrt{1 - \cos \omega t}} \quad \text{Equation A-49}$$

and the loss dissipated per unit of surface area is

$$P = z' \frac{J^2}{\sigma} = J_{speak}^2 \sqrt{\frac{B_s \omega}{\sigma}} \frac{\sin^2 \omega t}{\sqrt{1 - \cos \omega t}} \quad \text{Equation A-50}$$

and the average is

$$P_{avg} = \frac{4\sqrt{2}}{3\pi} J_{speak} \sqrt{\frac{B_s \omega}{\sigma}} \quad \text{Equation A-51}$$

Real and reactive components of the electric field due to the eddy currents can also be found. This will be useful in determining the power factor of the load. The electric field due to the flux within the magnetic material is

$$E = \sqrt{\frac{B_s \omega J_{speak}}{\sigma}} \left(\frac{\sin \omega t}{\sqrt{1 - \cos \omega t}} \right) \quad \text{Equation A-52}$$

in each half cycle. This can be written as

$$E = \sqrt{\frac{B_s \omega J_{speak}}{\sigma}} \cos\left(\frac{\omega t}{2}\right) \quad \text{Equation A-53}$$

The fundamental component is

$$E = \sqrt{\frac{B_s \omega J_{speak}}{\sigma}} \left[\frac{8}{3\pi} \sin \omega t + \frac{4}{3\pi} \cos \omega t \right] \quad \text{Equation A-54}$$

The phase angle between the electric field and the exciting current is

$$\theta = \tan^{-1}(0.5) = 26.6^\circ \quad \text{Equation A-55}$$

and the power factor is

$$\cos \theta = 0.895 \quad \text{Equation A-56}$$

A.2 Losses in Nonlinear Steel

To find the loss per square inch of surface, WPSI, use

$$WPSI = 1.51 \times 10^{-4} \sqrt{\rho_i B_s f H_p^3} \quad \text{Equation A-57}$$

Where ρ_i is the resistivity of the steel (Ω –in). B_s is the saturation flux density (if not known then recommend using 120,000 lines/in²). f is the frequency in Hertz. The value of H_p is the peak Amps/inch of the current sheet. If we have the current in the tooth, for example, then

$$H_p = \sqrt{2} \frac{I_m}{b_t} \quad \text{Equation A-58}$$

Where b_t is the tooth width and I_m is the tooth current.

We now compute the permeance and conductance for the equivalent circuit. The loss is the loss per square inch times the surface area and this also equals the current squared over the conductance.

$$WATTS = WPSI \times b_t \times (\text{unit depth}) = \frac{I_m^2}{G_i} \quad \text{Equation A-59}$$

So

$$WATTS = 2.54 \times 10^{-4} \sqrt{\frac{\rho_i B_s f}{b_t}} I_m^{\frac{3}{2}} \quad \text{Equation A-60}$$

If we call the coefficient and the square root K_ϕ then we have

$$G_i = \sqrt{\frac{I_m}{K_\phi}} \quad \text{Equation A-61}$$

From the theory section the reactance is 1/2 the resistance in the magnetic steel so that

$$X_i = \omega L_i = \omega P_i = \frac{R_i}{2} = \frac{1}{2G_i} \quad \text{Equation A-62}$$

Where P_i is the permeance (note that for one turn the inductance and permeances are the same).

$$P_i = \frac{1}{\omega} \frac{0.5}{G_i} \quad \text{Equation A-63}$$

We can check the formulation using a nonlinear finite element code (FLUX2D). In this case the current density is plotted from the rotor surface along a radial path (See Figure A-5). We see that the current decays swiftly as the depth increases and then goes to zero rather abruptly.

SIMPLE_SOLID093

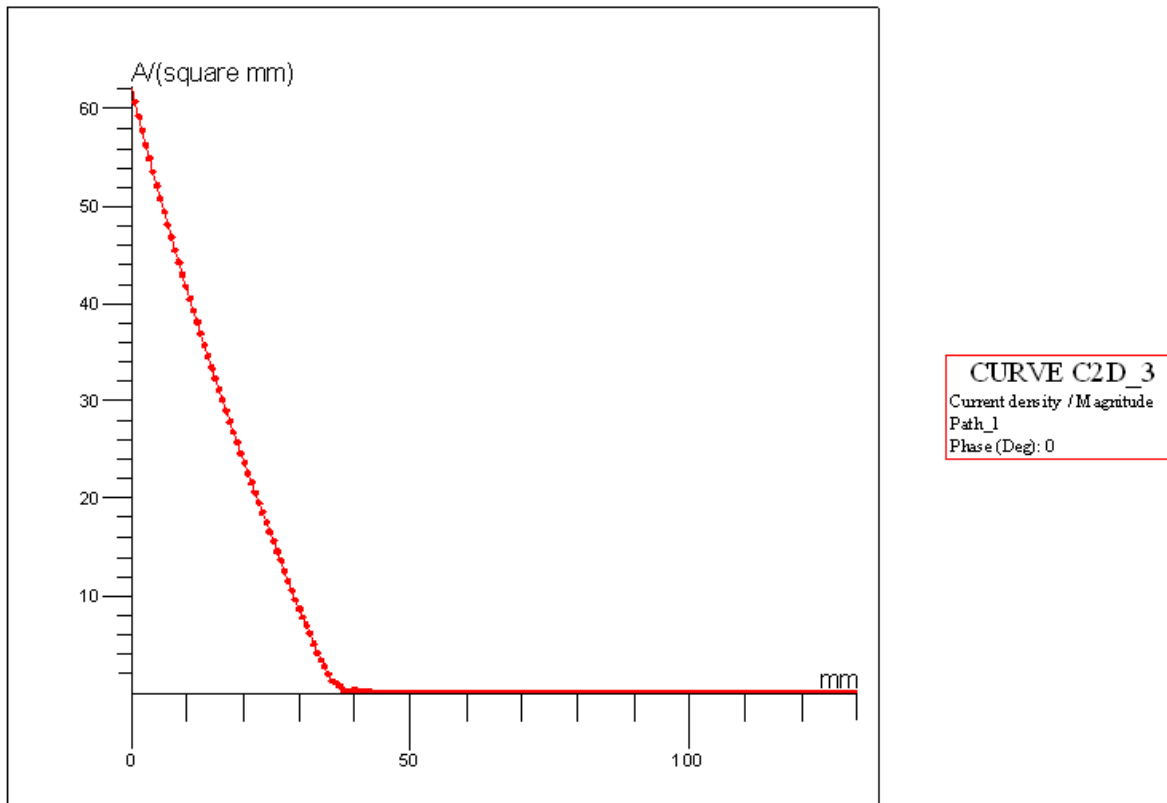


Figure A-5
Current density vs depth (low current)

This is what the nonlinear theory predicts. Figure A-5 is for 5,000 amperes. The skin depth, where the current goes to zero is around 35 mm. If we double the current we obtain the following solution (Figure A-6).

SIMPLE_SOLID186

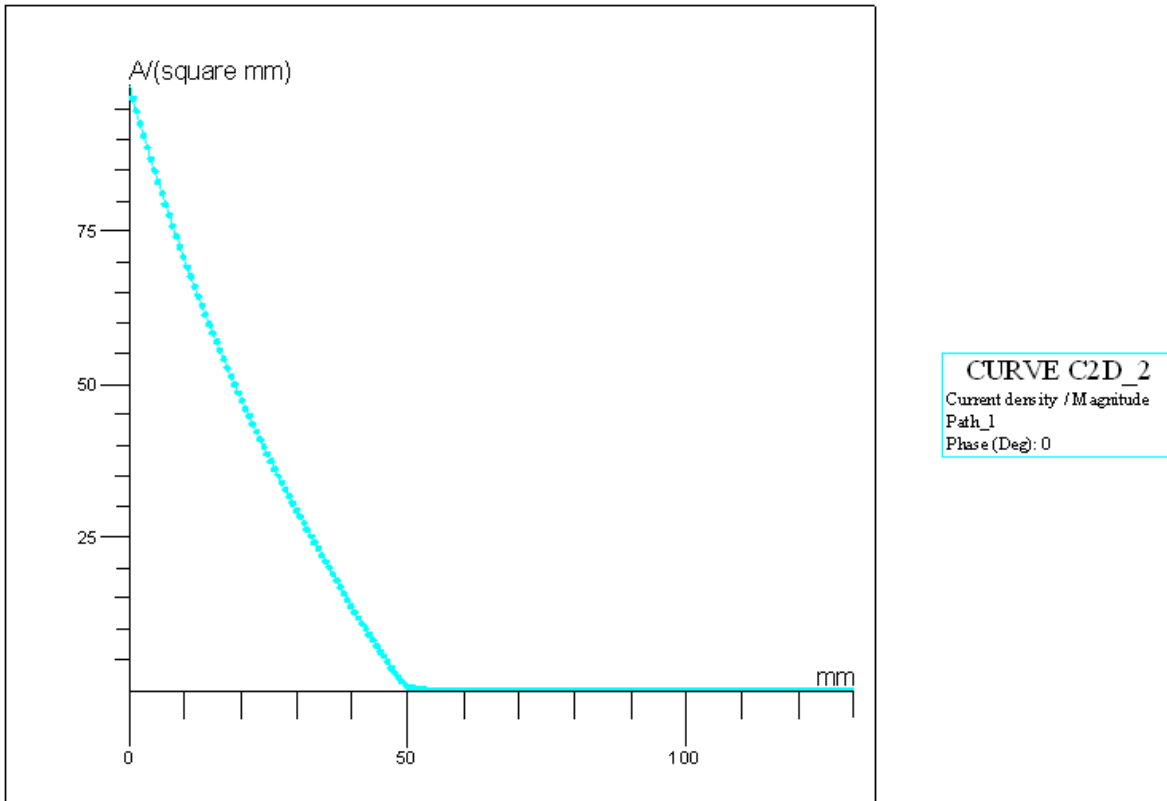


Figure A-6
Current density vs depth (medium current)

We see that the skin depth is approximately 50 mm. The limiting nonlinear theory tells us that the skin depth should vary proportional to the square root of the Amperes/in in the peripheral direction. This seems to be the case. If we now look at the results for 25,000 Amperes in Figure A-7, the skin depth appears to be around 73 mm. This is also in line with the nonlinear theory.

SIMPLE_SOLID465

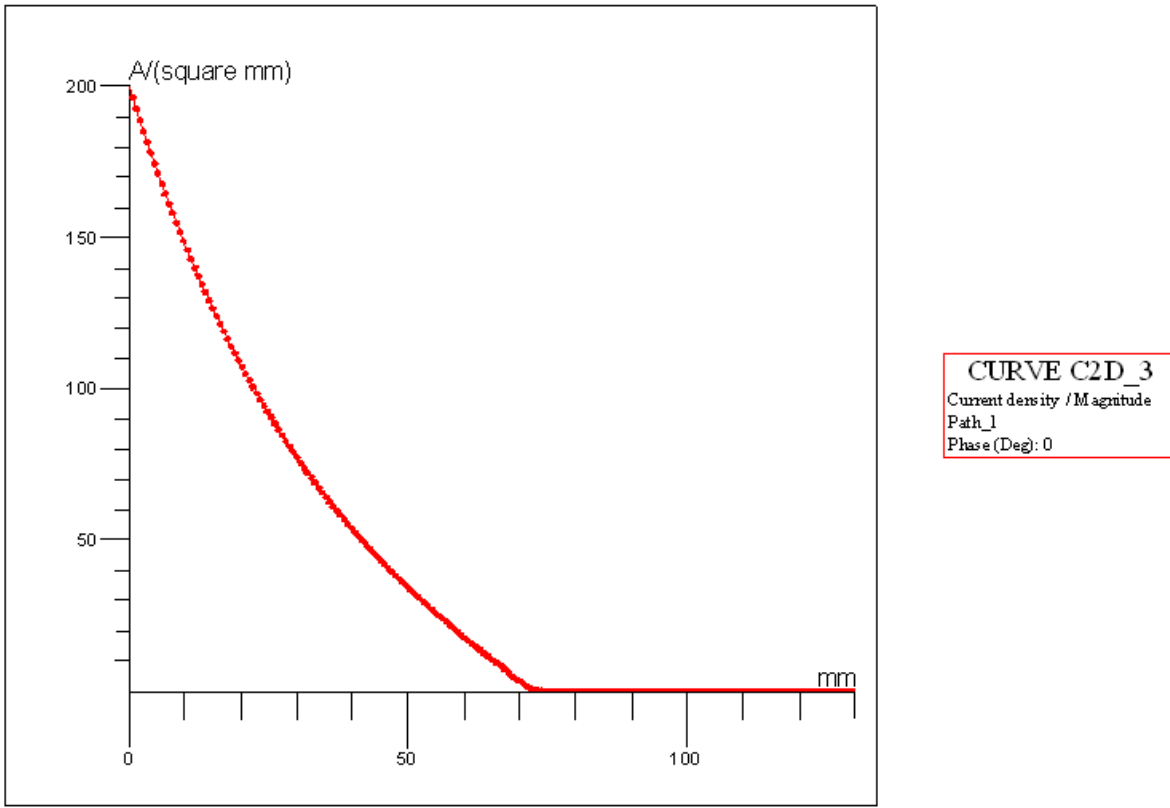


Figure A-7
Current density vs depth (high current)

Export Control Restrictions

Access to and use of EPRI Intellectual Property is granted with the specific understanding and requirement that responsibility for ensuring full compliance with all applicable U.S. and foreign export laws and regulations is being undertaken by you and your company. This includes an obligation to ensure that any individual receiving access hereunder who is not a U.S. citizen or permanent U.S. resident is permitted access under applicable U.S. and foreign export laws and regulations. In the event you are uncertain whether you or your company may lawfully obtain access to this EPRI Intellectual Property, you acknowledge that it is your obligation to consult with your company's legal counsel to determine whether this access is lawful. Although EPRI may make available on a case-by-case basis an informal assessment of the applicable U.S. export classification for specific EPRI Intellectual Property, you and your company acknowledge that this assessment is solely for informational purposes and not for reliance purposes. You and your company acknowledge that it is still the obligation of you and your company to make your own assessment of the applicable U.S. export classification and ensure compliance accordingly. You and your company understand and acknowledge your obligations to make a prompt report to EPRI and the appropriate authorities regarding any access to or use of EPRI Intellectual Property hereunder that may be in violation of applicable U.S. or foreign export laws or regulations.

The Electric Power Research Institute, Inc. (EPRI, www.epri.com) conducts research and development relating to the generation, delivery and use of electricity for the benefit of the public. An independent, nonprofit organization, EPRI brings together its scientists and engineers as well as experts from academia and industry to help address challenges in electricity, including reliability, efficiency, health, safety and the environment. EPRI also provides technology, policy and economic analyses to drive long-range research and development planning, and supports research in emerging technologies. EPRI's members represent more than 90 percent of the electricity generated and delivered in the United States, and international participation extends to 40 countries. EPRI's principal offices and laboratories are located in Palo Alto, Calif.; Charlotte, N.C.; Knoxville, Tenn.; and Lenox, Mass.

Together...Shaping the Future of Electricity

Program:

Steam Turbines, Generators, and Balance-of-Plant

© 2009 Electric Power Research Institute (EPRI), Inc. All rights reserved. Electric Power Research Institute, EPRI, and TOGETHER...SHAPING THE FUTURE OF ELECTRICITY are registered service marks of the Electric Power Research Institute, Inc.

 Printed on recycled paper in the United States of America

1015671

Electric Power Research Institute

3420 Hillview Avenue, Palo Alto, California 94304-1338 • PO Box 10412, Palo Alto, California 94303-0813 USA
800.313.3774 • 650.855.2121 • askepri@epri.com • www.epri.com